

1
2
3
4
5
6
7
8
9
10
11
12
13
14
15
16
17
18
19
20
21

**Heterogeneous Interactions between SO₂ and
Organic Peroxides in Submicron Aerosol**

Shun Yao Wang¹, Tengyu Liu², Jinmyung Jang¹,
Jonathan P.D. Abbatt² and Arthur W.H. Chan^{1*}

¹ Department of Chemical Engineering and Applied Chemistry, University of Toronto,
Toronto, Ontario, M5S 3E5, Canada

² Department of Chemistry, University of Toronto, Toronto, Ontario, M5S 3H6, Canada

**Correspondence to:* Arthur W.H. Chan (arthurwh.chan@utoronto.ca)

22 **Abstract**

23 Atmospheric models often underestimate particulate sulfate, a major component in ambient
24 aerosol, suggesting missing sulfate formation mechanisms in the models. Heterogeneous
25 reactions between SO₂ and aerosol play an important role in particulate sulfate formation and its
26 physicochemical evolution. Here we study the reactive uptake kinetics of SO₂ onto aerosol
27 containing organic peroxides. We present chamber studies of SO₂ reactive uptake performed
28 under different relative humidities (RH), particulate peroxide contents, peroxide types, and
29 aerosol acidities. Using different model organic peroxides mixed with ammonium sulfate
30 particles, SO₂ uptake coefficient (γ_{SO_2}) was found to be exponentially dependent on RH. γ_{SO_2}
31 increases from 10⁻³ at RH 25% to 10⁻² at RH 71% as measured for an ~~an~~-multifunctional-organic
32 peroxide with multiple O-O groups. Under similar conditions, the kinetics in this study were
33 found to be structurally dependent: ~~multifunctional~~-organic peroxides with multiple peroxide
34 groups have a higher γ_{SO_2} than those with only one peroxide group, consistent with the reactivity
35 trend observed previously in the aqueous phase. In addition, γ_{SO_2} is linearly related to particle-
36 phase peroxide content, which in turn depends on gas-particle partitioning of organic peroxides.
37 Aerosol acidity plays a complex role in determining SO₂ uptake rate, influenced by the effective
38 Henry's Law constant of SO₂ and the condensed phase kinetics of the peroxide-SO₂ reaction in
39 the highly concentrated aerosol phase. These uptake coefficients are consistently higher than
40 those calculated from the reaction kinetics in the bulk aqueous phase, and we show experimental
41 evidence suggesting that other factors, such as particle-phase ionic strength, can play an essential
42 role in determining the uptake kinetics. γ_{SO_2} for different types of secondary organic aerosol
43 (SOA) were measured to be on the order of 10⁻⁴. Overall, this study provides quantitative

44 evidence of the multiphase reactions between SO₂ and organic peroxides, highlighting the
45 important factors that govern the uptake kinetics.

46 **Introduction**

47 Sulfate and organic compounds are ubiquitous particulate components in both polluted and
48 pristine environments (Chen et al., 2009;Andreae et al., 2018;He et al., 2011;Sun et al.,
49 2013;Huang et al., 2014), with important implications for public health and global climate
50 (Hallquist et al., 2009). Particulate sulfate can form via S(IV) oxidation by OH radicals in the gas
51 phase and via oxidation in cloud water, fog droplets or the aerosol aqueous phase, including by
52 H₂O₂, O₂ (catalyzed by transition metals), O₃, NO₂ and small organic peroxides (methyl
53 hydroperoxide and peroxyacetic acid) (Seinfeld and Pandis, 2012). However, atmospheric
54 models tend to underestimate particulate sulfate production on both global (Tie et al., 2001;Yang
55 et al., 2017;Fairlie et al., 2010) and regional scales, especially during heavy haze episodes (Wang
56 et al., 2014;Zheng et al., 2015;Sha et al., 2019;Gao et al., 2016;Li et al., 2017;Huang et al.,
57 2019), suggesting that the overall kinetics may be underestimated and/or important mechanisms
58 may be missing in models.

59 To reconcile these differences, studies have investigated novel reaction mechanisms of sulfate
60 formation. Stabilized Criegee intermediates (sCIs) were ~~hypothesized~~found to oxidize SO₂
61 rapidly and ~~proposed to be~~potentially serve as an important source of ambient sulfate (Mauldin et
62 al., 2012). In the work by Newland et al. (2015) and Nguyen et al. (2016), this sCI pathway was
63 shown to play a minor role in sulfate formation. More recently, when Liu et al. (2019) applied
64 this mechanism and kinetics to a source-oriented WRF-Chem model, the sCIs pathway was
65 found to only account for at most 9% of the total particulate sulfate. Reactive nitrogen species
66 (such as NO₂) have also been proposed as a dominant sulfate formation pathway when aerosol

67 pH was estimated to be 5-6 in Cheng et al. (2016) and close to 7 in Wang et al. (2016) under
68 severe haze scenarios. Reactive nitrogen species (such as NO₂) have also been put forward to
69 account for the missing sulfate at relatively high aerosol pH (close to 7) (Wang et al.,
70 2016; Cheng et al., 2016). However, While such high aerosol pH is not substantiated by some
71 thermodynamic modeling resultss, which concluded that pH ranges between 4 and 5 even in
72 polluted regions (Song et al., 2018; Guo et al., 2017), other studies that highlighted the roles of
73 ammonia and dust found aerosol pH could be higher than 6 (Shi et al., 2017; Ding et al., 2019).-
74 Furthermore, higher aerosol water content and PM mass concentration in polluted areas have
75 been shown to enhance the aerosol pH via a multiphase buffering process (Zheng et al., 2020).
76 Meanwhile, a recent modeling study incorporating this heterogeneous NO_x mechanism still
77 exhibited a discrepancy of 20% between the predicted and observed sulfate, indicating the
78 possibility of unknown mechanisms (Huang et al., 2019). Other factors may play a role in
79 enhancing the particle-phase sulfate formation rates. Chen et al. (2019) investigated the
80 synergistic effects of NO₂ and NH₃ on sulfate formation, and found that the rate of this reaction
81 can be enhanced by the high ionic strength in the particle phase. This enhancement effect by
82 solute strength on sulfate formation was also investigated for the H₂O₂ pathway in aerosol liquid
83 water. Liu et al. (2020) found ionic strength and general acid-catalyzed mechanisms can cause
84 the S(VI) formation rate to be nearly 50 times faster in aerosol phase than in dilute solutions. On
85 the other hand, during the severe haze episodes in China (Li et al., 2020; Guo et al., 2017),
86 transition metal ion (TMI) catalysis of SO₂ oxidation by O₂ can be significantly suppressed in the
87 aerosol phase due to high ionic strength (Liu et al., 2020; Cheng et al., 2016; Su et al., 2020).
88 In addition to high solute strength, submicron aerosol is also rich in organic compounds (Jimenez
89 et al., 2009; Hallquist et al., 2009). In recent years, many studies have investigated the potential

90 role of heterogeneous interactions between SO₂ and organic aerosol on particulate sulfate
91 formation. Song et al. (2019) found heterogeneous oxidation of hydroxymethanesulfonate
92 (HMS) by OH can trigger rapid sulfate formation. Wang et al. (2020) studied photosensitizers in
93 ambient particles and found this pathway could be essential under specific light conditions.
94 Recent studies found reactive intermediates from isoprene oxidation (Huang et al., 2019) and
95 benzoic acid (Huang et al., 2020), can yield a variety of organosulfur species upon catalysis by
96 TMI. Other studies have also investigated the interactions between secondary organic aerosol
97 (SOA) and SO₂. Field observations found that ambient sulfate abundance is highly correlated
98 with SOA formation (Yee et al., 2020; Xu et al., 2015). Liu et al. (2019) found that SO₂ enhances
99 SOA formation and average carbon oxidation state during methoxyphenol photooxidation. By
100 performing chamber experiments with limonene SOA formation in the presence of SO₂, Ye et al.
101 (2018) also observed significant SO₂ decay along with increased SOA yields and carbon
102 oxidation state, proposing that organic peroxides in SOA may be the key reactive intermediates
103 for SO₂ oxidation.

104 Organic peroxides are key intermediates for aerosol formation and ubiquitously exist in many
105 SOA systems (Hallquist et al., 2009; Bianchi et al., 2019). Numerous studies have reported
106 peroxide content of 20-60% for isoprene and monoterpene derived SOA (Surratt et al., 2006; Ng
107 et al., 2008; Ye et al., 2018; Epstein et al., 2014). A significant fraction of organic peroxide (30%-
108 50%) has also been found in naphthalene-derived SOA under low/high NO_x conditions
109 (Kautzman et al., 2009). Using model simulations, Bonn et al. (2004) found organic
110 hydroperoxides can account for up to 60% of global SOA. The aqueous phase reaction kinetics
111 between organic peroxides and dissolved SO₂ have been explored in previous studies (Lind et al.,
112 1987; Gunz and Hoffmann, 1990; Wang et al., 2019; Dovrou et al., 2019; Yao et al., 2019). The

113 second order reaction rate constants for organic peroxides in SOA (Dovrou et al., 2019; Yao et
114 al., 2019) and S(IV) were measured to be on the order of 10^2 - 10^3 $M^{-1} s^{-1}$, which are within the
115 range of those measured for commercially available organic peroxides (Wang et al., 2019) and
116 small organic peroxides (Lind et al., 1987). Yao et al. (2019) quantified the reactive uptake
117 coefficient of SO_2 (γ_{SO_2}) onto α -pinene SOA to be on the order of 10^{-4} - 10^{-3} , which is positively
118 dependent on RH and inferred particle-phase peroxide content. These reactions are also linked to
119 the formation of organosulfates (Wang et al., 2019). Both inorganic sulfate (85-90%) and
120 organosulfates (10-15%) were observed as products of SO_2 reactive uptake onto SOA (Yao et al.,
121 2019).

122 Given the potential significance of SO_2 reactive uptake in particulate sulfate formation, a more
123 in-depth study is needed to determine the important factors that govern the heterogeneous
124 kinetics of SO_2 onto organic peroxide containing aerosol. In this study, we measured γ_{SO_2} for two
125 categories of aerosol: 1. Model organic peroxides mixed with ammonium sulfate or malonic acid
126 and 2. SOA from a few representative biogenic and anthropogenic precursors. The impacts of
127 RH, peroxide type, peroxide content, and condensed phase pH on SO_2 reactive uptake were
128 evaluated systematically with the goal of better understanding atmospheric multiphase sulfate
129 formation.

130

131 **2. Methods**

132 The reactive uptake of SO_2 onto peroxide-containing particles was studied in a 1 m^3 Teflon
133 chamber under ambient temperature and pressure. In brief, generated particles and SO_2 were
134 introduced into the chamber separately. The consumption of SO_2 , changes in particle size

135 distribution and chemical composition were monitored to estimate the reactive uptake
136 coefficients. Particles were also collected on filters for offline chemical characterization.

137

138 **2.1 Seed aerosol generation**

139 In this work, two types of aerosol were used to investigate the uptake of SO₂. The first is
140 ammonium sulfate or malonic acid mixed with model organic peroxides (Fig. S1). In this first set
141 of experiments, an aerosol atomizer (Model 3076, TSI Inc., USA) was used to generate aqueous
142 particles from dilute solution. Each solution consists of ammonium sulfate ($\geq 99\%$, Sigma-
143 Aldrich) or malonic acid (99%, Sigma-Aldrich) and a model organic peroxide in ultrapure water
144 (HPLC grade, Fisher Chemical). For the experiments investigating the relationship between γ_{SO_2}
145 and peroxide type (Expt. 2-14, [Table S1](#)), different commercially available organic peroxides
146 were used, including tert-butyl hydroperoxide (70 wt. % in water, Sigma-Aldrich), cumene
147 hydroperoxide (80 wt. % in water, Sigma-Aldrich), and 2-butanone peroxide (40% wt. % in
148 water, Sigma-Aldrich). The molar ratio of organic peroxide to ammonium sulfate in the
149 atomizing solution was 2:1 with the aim of being atmospherically relevant (corresponding to
150 maximum particulate peroxide molar fraction of 66% and mass fraction of approximately 50-
151 70% if all the organic peroxides were assumed to remain in the particle phase). This ratio was
152 used as a proxy for total peroxide content in both gas and particle phase relative to that of
153 ammonium sulfate upon atomization. For the experiments studying the relationship between γ_{SO_2}
154 and particle-phase peroxide content, the molar ratio of organic peroxide to ammonium sulfate
155 (Expt. 10-12, 15-18, [Table S1](#)) in the solution was adjusted to be 0.02, 0.2, 1, 2, and 4,
156 respectively. In experiments where malonic acid was used (Expt. 19-22, [Table S1](#)), molar ratios
157 of 0.2, 1, 2, and 4 were adopted. For measuring γ_{SO_2} with different aerosol pH (Expt. 17, 23-25,

158 [Table S1](#)), different amounts of HCl (37%, Sigma-Aldrich) were added into the solution ([0.](#)
159 [0.00002 M, 0.0001 M, 0.001 M HCl](#)) prior to atomization. [The initial pH of aerosol \(2.5, 2.2,](#)
160 [1.6, 1, respectively\)](#) were modeled using E-AIM III model (Clegg et al., 1998) based on the
161 [initial molar ratios of inorganic species \(\$H^+\$, \$NH_4^+\$, \$SO_4^{2-}\$, \$Cl^-\$ \) in the atomizing solution and](#)
162 [measured RH \(around 50%\)](#). The atomized particles were flowed into the chamber without
163 drying, and therefore assumed to remain deliquesced under the range of RH we studied. Expt. 2-
164 14 ([Table S1](#)) also represent those where the relationship between γ_{SO_2} and RH conditions were
165 studied.

166 In the second set of experiments, the uptake of SO_2 onto SOA was investigated (Fig. S2, Expt.
167 26-28, [Table S1](#)). A custom-built 10 L quartz oxidation flow reactor was used to produce SOA
168 (Ye et al., 2016) from different hydrocarbon precursors. In this work, we studied SOA formed
169 from toluene photooxidation, limonene ozonolysis and α -pinene ozonolysis, 3 of the most
170 commonly studied SOA systems (Ng et al., 2007; Hildebrandt et al., 2009; Hartz et al.,
171 2005; Varutbangkul et al., 2006). Toluene (analytical standard, Sigma Aldrich) was injected
172 continuously into zero air flow by a syringe (1000 mL, Hamilton) installed on a syringe pump
173 (KDS Legato100) to achieve an initial concentration of 0.5 ppm. Limonene (Sigma-Aldrich,
174 97 %) and α -pinene (Sigma-Aldrich, 98 %) were pre-dissolved in cyclohexane (Sigma-Aldrich,
175 99.5 %) with a volumetric ratio of 1: 1500 and 1: 500 to ensure that OH formed from limonene
176 or α -pinene ozonolysis is scavenged by cyclohexane, estimated based on the rate constants
177 (Atkinson and Arey, 2003). The initial steady-state concentrations of limonene and α -pinene
178 were controlled to be around 2 ppm and 1 ppm entering the flow tube. O_3 , used as the oxidant
179 (for limonene and α -pinene) or the OH precursor (for toluene), was generated by passing 0.5 L
180 min^{-1} pure oxygen (99.6 %, Linde, Mississauga, Canada) through an O_3 generator (no.

Formatted: Superscript

Formatted: Subscript

Formatted: Superscript

Formatted: Subscript

Formatted: Superscript

Formatted: Superscript

181 97006601, UVP, Cambridge, UK). Humidified air was produced by bubbling zero air through a
182 custom-made humidifier at a flow rate of 1 L min⁻¹. The photolysis of O₃ produces O (¹D),
183 which reacts with water vapour to produce ·OH with illumination from the 254 nm UV lamps
184 (UVP, Cambridge, UK) to initiate the photooxidation of toluene. The average residence time
185 inside the flow tube was controlled to be around 5 minutes. A gas chromatography–flame
186 ionization detector (GC-FID, model 8610C, SRI Instruments Inc., LV, USA) equipped with a
187 Tenax® TA trap was used to monitor the concentration of hydrocarbon precursors at the
188 inlet/outlet of the flow reactor. In all cases, the O₃ concentration was maintained to be at least 10
189 times higher than that of the hydrocarbon. Temperature and relative humidity were monitored by
190 an Omega HX94C RH/T transmitter. Particle size distribution and volume concentration were
191 monitored using a custom-built scanning mobility particle sizer (SMPS), which is a combination
192 of a differential mobility analyzer column (DMA, model 3081, TSI, Shoreview, MN, USA) with
193 flow controls and a condensation particle counter (CPC, model 3772, TSI, Shoreview, MN,
194 USA).

195

196 **2.2 Quantification of γ_{SO_2}**

197 Prior to each experiment, the chamber was flushed by purified air overnight with a flow rate of
198 25 L min⁻¹ until particle number concentration was less than 5 cm⁻³ and SO₂ was less than 1 ppb.
199 To adjust RH, the chamber was humidified by passing purified air through a custom-built
200 humidifier filled with ultra-pure water. For experiments with atomized ammonium sulfate or
201 malonic acid, SO₂ was injected into the chamber prior to the introduction of particles. For
202 experiments studying γ_{SO_2} onto SOA, aerosol generated from the flow tube was injected into the
203 Teflon chamber continuously after passing through an O₃ denuder (Ozone Solutions, Iowa, USA)

204 to achieve specific aerosol concentration inside the chamber prior to SO₂ addition. SO₂ mixing
205 ratio in the chamber during each experiment was continuously monitored using an SO₂ analyzer
206 (Model 43i, Thermo Scientific). The initial mixing ratio of SO₂ in each experiment was
207 controlled to be around 200 ppb. Aerosol size distribution was monitored by SMPS. The reactive
208 uptake coefficient of SO₂ was calculated by integrating the following equation:

$$209 \quad -\frac{d[SO_2]}{dt} = \frac{1}{4}\gamma_{SO_2}A\bar{c}[SO_2] \quad (1)$$

210 Where [SO₂] is the SO₂ mixing ratio (ppb) monitored by the SO₂ analyzer; A is the average
211 surface area concentration (μm² cm⁻³) derived from the particle size distribution measured by
212 SMPS; \bar{c} represents the mean molecular velocity (cm s⁻¹) of SO₂. d[SO₂]/dt is solved over the
213 initial SO₂ decay, such that the peroxide concentration in the aerosol liquid phase is assumed to
214 be constant and pseudo-first order kinetics can be applied (Abbatt et al., 2012; Thornton et al.,
215 2003). A summary of all the measured γ_{SO_2} can be found in Table S1. Typical evolution of
216 monitored species can be seen in Fig.1. Control experiments were performed in order to rule out
217 other potential factors (e.g. SO₂ loss in the in-line filter in front of the SO₂ analyzer, interferences
218 inside the SO₂ analyzer, chamber wall losses, SO₂ uptake onto wet ammonium sulfate, gas-phase
219 reaction of SO₂ with peroxide vapour) that may contribute to the SO₂ decay observed during the
220 γ_{SO_2} measurement inside the chamber (Fig. S3-S6). Measurement uncertainty and precision of
221 γ_{SO_2} in this study can be found in Table S1. Also, we observed there was SO₂ repartitioning from
222 the humid chamber wall in the presence of organic peroxide under high RH (Fig. S6b, RH 74%).
223 The observed SO₂ repartitioning rate was then applied to correct the γ_{SO_2} measured under high
224 RH conditions (above 70%, Expt.14), and this correction amounts to a 40% increase in
225 calculated γ_{SO_2} .
226
227

228 2.3 Offline peroxide quantification

229 Aerosol was collected onto 47 mm PTFE (polytetrafluoroethylene) filters with 0.2 μm pore size
230 (Whatman®, GE Healthcare) from the chamber by a diaphragm pump (KNF Neuberger Inc., USA)
231 for offline chemical analysis. The total particulate peroxide content (H₂O₂, ROOH and ROOR) in
232 these samples prior to SO₂ uptake was quantified using the iodometric–spectrophotometric assay
233 (Docherty et al., 2005). I₂ produced from the reaction between I⁻ and peroxides can further quickly
234 combine with the excess amount of I⁻ to form I₃⁻, which has brown color and absorbs UV-vis at
235 470nm. The SOA extraction was then aliquoted into a 96-well UV plate (Greiner Bio-One,
236 Kremsmünster, AT) with 160 μL well⁻¹. 20 μL of formic acid (≥ 95 %, Sigma-Aldrich) was added
237 into each well, following by 20 μL potassium iodide (BioUltra, ≥99.5%, Sigma-Aldrich) solution
238 (dissolved in DI water). The plate was then covered by an adhesive plate sealer (EdgeBio,
239 Gaithersburg, USA) immediately in order to avoid reagent evaporation and O₂ oxidation. After
240 incubation for an hour in the dark, the UV-vis absorption at 470nm was measured using a UV-vis
241 spectrophotometer (Spectramax 190, Molecular Devices Corporation, Sunnyvale, CA) and then
242 converted to peroxide concentration using the calibration curve made by tert-butyl hydroperoxide
243 (70 wt. % in H₂O, Sigma-Aldrich) with a series of concentrations (0-10mM). An average
244 molecular mass for seed particles (SOA + ammonium sulfate) was assumed based on the chemical
245 composition in order to calculate the molar fraction of total peroxides using the following equation:

$$\text{Molar fraction of peroxide} = \frac{N_{\text{peroxide}}}{N_{\text{aerosol}}} = \frac{N_{\text{peroxide}} \cdot M_{(\text{NH}_4)_2\text{SO}_4} \cdot f_{(\text{NH}_4)_2\text{SO}_4} + M_{\text{peroxide}} \cdot f_{\text{peroxide}}}{m_{\text{aerosol}}} \quad (2)$$

248 where m_{aerosol} is the weighed aerosol mass on the filter; $M_{(\text{NH}_4)_2\text{SO}_4}$ and M_{peroxide} are the
249 molecular mass of ammonium sulfate and peroxide, respectively; $f_{(\text{NH}_4)_2\text{SO}_4}$ and f_{peroxide} are the
250 initial molar fraction of ammonium sulfate and peroxide; N_{peroxide} and N_{aerosol} are the

Formatted: Line spacing: Double

Formatted

Formatted: Font color: Text 1

Formatted

Formatted

Formatted

Formatted

Formatted

Formatted

Formatted

Formatted

Formatted

252 ~~measured peroxide molar and calculated aerosol molar, respectively. The average molecular~~
253 ~~mass for aerosol was assumed based on the chemical composition in order to calculate the molar~~
254 ~~fraction of total peroxides.~~ More details about the iodometric-spectrophotometric procedures
255 were described in previous work (Wang et al., 2018).

Formatted: English (Canada)

257 **3 Results and discussion**

258 **3.1 SO₂ uptake and RH**

259 A positive relationship between γ_{SO_2} and RH (between 25 and 71%) was observed for all types of
260 organic peroxides studied (Fig. 2). The positive dependence of the reactive uptake coefficient of
261 water-soluble gaseous species on RH has also been observed in other studies (Thornton et al.,
262 2003;Griffiths et al., 2009;Zhao et al., 2017;Zhang et al., 2019). Recently, the uptake behavior of
263 SO₂ onto soot, mineral dust and SOA were also shown to positively depend on RH (Zhang et al.,
264 2019;Zhao et al., 2017;Yao et al., 2019).

265 It is also noteworthy that an exponential dependence of SO₂ reactive uptake coefficient on RH
266 was observed in our study. γ_{SO_2} increases with increased relative humidity, which could even be
267 more significant under high RH regime. This is consistent with previous laboratory studies that
268 measured the reactive uptake coefficient of SO₂ onto aerosol to be exponentially dependent on
269 RH (Zhang et al., 2019;Yao et al., 2019). Additionally, multiple field campaigns have observed
270 significant correlation between particulate sulfate formation and ambient RH (Song et al.,
271 2019;Sun et al., 2013;Huang et al., 2020). Sun et al. (2013) observed faster sulfate formation rate
272 under humid conditions, proposing a significant impact of aerosol liquid water on sulfate
273 production during wintertime in Beijing. Zheng et al. (2015) reported a notably higher SOR
274 (molar ratio of sulfate to the sum of sulfate and SO₂) during wet period (RH>50%), indicating

275 the importance of heterogeneous reactions to the secondary sulfur transformation with abundant
276 aerosol water content under humid conditions. In a recent study by Song et al. (2019), the rapid
277 sulfate formation rate observed under high RH conditions was found to be significantly higher
278 than atmospheric modeling results implemented with homogeneous SO₂ oxidation pathways,
279 which was later attributed to heterogeneous sulfate formation mechanisms. Multiple mechanisms
280 can potentially explain this observed γ_{SO_2} -RH dependence. An enhanced relative humidity would
281 result in a nonlinear increase of aerosol water content, which can lead to more SO₂ dissolved in
282 the aerosol aqueous phase (Seinfeld and Pandis, 2012). It should be noted that while the relative
283 humidity is varied systematically in these experiments, the relationship is more complex since
284 RH also affects other aerosol properties which can affect the uptake kinetics in turn. For
285 example, a higher aerosol liquid water content could dilute protons and thus lower the aerosol
286 acidity. In a study by Laskin et al. (2003), an enhanced uptake of SO₂ onto sea-salt particles was
287 observed with an increased aerosol alkalinity at high pH range.

288 289 **3.2 Dependence of SO₂ uptake on peroxide content and type**

290 As expected, the measured uptake rate of SO₂ is dependent on the particulate peroxide content in
291 the current study. Fig. 3 shows that γ_{SO_2} is linearly proportional to the amount of particulate
292 peroxide for aerosol with similar volume-to-surface ratios and containing the same type of
293 organic peroxides. This positive relationship between γ_{SO_2} and condensed phase peroxide content
294 has also been inferred from experiments of SO₂ uptake onto α -pinene SOA (Yao et al., 2019),
295 where the peroxide content in α -pinene SOA was varied indirectly by introducing NO and
296 adjusting the branching ratio of the peroxide-yielding RO₂+HO₂/RO₂ pathway.

297 In addition to the amount of peroxide injected, the particulate fraction of organic peroxide
298 available for heterogeneous reaction is also influenced by gas-particle partitioning. As indicated
299 in Fig. 2, the reactive uptake coefficients of different organic peroxides vary amongst each other
300 by about an order of magnitude in the range of RH studied, despite the same amounts of peroxide
301 relative to ammonium sulfate initially in the atomizing solution. Based on our previous work
302 (Wang et al., 2019), the aqueous-phase rate constants for these organic peroxides with dissolved
303 S(IV) only vary by a factor of 2-3 and therefore cannot fully explain the observed difference in
304 uptake rates. Since vapour pressure vary considerably among the different peroxides in the
305 present study, gas-particle partitioning is likely to influence the amount of peroxide in the
306 particle phase that react with dissolved SO₂. The relative particulate peroxide content on filters
307 of the three peroxides collected from chamber experiments under RH 50% without SO₂ uptake
308 were measured by the offline KI method (Fig. S7). Although the initial ratio of organic peroxide
309 to ammonium sulfate in the atomizing solution was nominally the same, we measured the highest
310 amount of particulate peroxide with 2-butanone peroxide (16.7%), followed by cumene
311 hydroperoxide (12.7%) and then tert-butyl hydroperoxide (3.8%) using the offline iodometric
312 method. This trend in particulate peroxide content is consistent with the vapour pressures
313 calculated using the SIMPOL group contribution method (Pankow et al., 2008), with 2-butanone
314 peroxide being the least volatile, and tert-butyl hydroperoxide being the most volatile. Also, the
315 order of particle-phase peroxide content is consistent with the order of γ_{SO_2} observed, as shown in
316 Fig. 2. A simple visualization of these relationships between different peroxide characteristics
317 (number of peroxide groups, vapour pressure and aqueous-phase rate constants) and measured
318 γ_{SO_2} (at RH = 50%) is illustrated in Fig. S7, which indicates higher γ_{SO_2} can be expected for
319 ~~multifunctional~~ organic peroxides with multiple O-O groups. ~~with~~ lower vapour pressures and

320 higher aqueous phase reactivities. It should be noted that the order of magnitude difference in
321 experimentally measured γ_{SO_2} among various organic peroxides (Fig.2) is still not fully explained
322 when both volatility and reaction kinetics are taken into account (Fig.S7), suggesting that the
323 reactive uptake may be influenced by other factors. In summary, for our current experiments
324 where we nominally maintained total injected amount of organic peroxide constant, measured
325 γ_{SO_2} depends both on reactivity and gas-particle partitioning of the organic peroxides.

326

327 **3.3 SO₂ uptake and aqueous phase kinetics**

328 Since the aqueous phase reaction rate constants between S(IV) and these model organic
329 peroxides have been measured previously (Wang et al., 2019), we can test our understanding of
330 the measured γ_{SO_2} using a simple model. By assuming the amount of SO₂ dissolved in the aerosol
331 is in equilibrium with the gas phase, the overall γ_{SO_2} can be expressed using the simplified
332 resistor model (Hanson et al., 1994):

333

$$334 \quad \frac{1}{\gamma} = \frac{1}{\alpha} + \frac{\bar{c}}{4HRT\sqrt{k^I D_1}} \frac{1}{\left[\coth(q) - \frac{1}{q}\right]} \quad (3)$$

335 where α is the mass accommodation coefficient, \bar{c} is the mean molecular speed of SO₂ (cm s⁻¹),
336 H is the effective Henry's law constant that includes both the dissolution of SO₂ and the
337 dissociation of H₂SO₃ (M atm⁻¹), R is the ideal gas constant (atm L mol⁻¹ K⁻¹), T is the
338 temperature (K), and the parameter q is used to describe the competition between the reaction
339 and diffusion of the dissolved gaseous species within a particle, which is further calculated as:

$$340 \quad q = r \sqrt{\frac{k^I}{D_1}} \quad (4)$$

341 where r is the radius (cm) of a given particle, D₁ is the aqueous-phase diffusion coefficient (cm²
342 s⁻¹), k^I is the first order rate constant (s⁻¹) for the reaction. For experiments in the current study,

343 the calculated q values were consistently found to be far less than 1, which indicates a volume-
344 limited reaction regime. Combining with the assumption of a relatively fast mass
345 accommodation process compared with the bulk phase reaction, equation (3) can be further
346 simplified as to describes reactive uptake in the volume-limited regime:

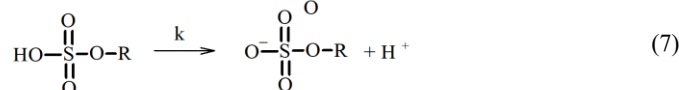
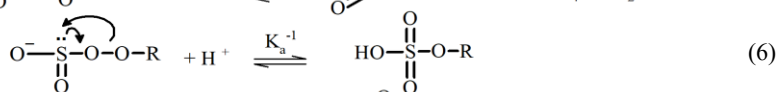
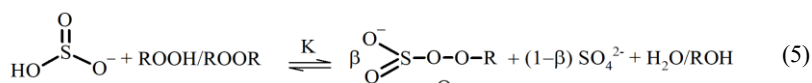
$$347 \quad \gamma = \frac{4HRT[\text{peroxide}]k^{\text{II}}V}{\bar{c}S} \quad (5)$$

348 Here, we assume all the peroxides remain in the condensed phase upon atomizing and reaction
349 inside the chamber for the upper-bound prediction of γ_{SO_2} . [peroxide] represents the particle phase
350 concentration of total organic peroxide (M) based on the initial ratio between organic peroxide and
351 ammonium sulfate in the atomizing solution, and the aerosol water content output by E-AIM III
352 (Clegg et al., 1998), k^{II} is the second order reaction rate constant ($\text{M}^{-1} \text{s}^{-1}$), which we have
353 measured in the bulk phase at dilute concentrations previously (Wang et al., 2019), V/S is the ratio
354 between particle volume concentration ($\mu\text{m}^3 \text{cm}^{-3}$) and particle surface area concentration (μm^2
355 cm^{-3}) derived from SMPS measurements. As a result, the observed reactive uptake coefficient of
356 SO_2 can be compared to that predicted from the bulk phase reaction rate constant, and the results
357 are shown in Fig. 4 and Fig. S8. Overall, we noticed that this model captures the dependence of
358 γ_{SO_2} on peroxide content, but the modeled results were found to be generally 15-50 times lower
359 than the experimentally measured values (Fig. S8). The current γ_{SO_2} predictions are likely upper-
360 bound estimates since all the peroxides were assumed to stay in the condensed phase without
361 partitioning. As a result, this observed 15-50 times of discrepancy could even be larger if the
362 particulate peroxide content during the chamber experiments were lower due to partitioning.

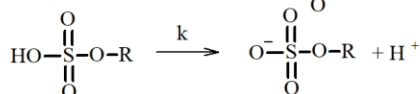
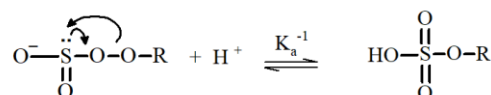
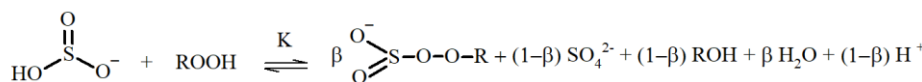
363 It should be noted that the calculated γ_{SO_2} was based on reaction kinetics measured in dilute
364 solutions while the experimental γ_{SO_2} were measured directly from suspended particles. This large
365 difference in kinetics between those in aerosol and in dilute bulk solution suggests that this

366 multiphase interaction is strongly favored in the highly concentrated aerosol environment. One of
367 the potential explanations for this discrepancy could be liquid-liquid phase separation (LLPS) in
368 aerosol between organic peroxide and ammonium sulfate (Ciobanu et al., 2009; O'Brien et al.,
369 2015) such that SO₂ can directly interact with the acidic organic phase, where the concentration of
370 peroxides can be higher and the kinetics can be different from what we have measured in dilute
371 solution (Wang et al., 2019). However, LLPS is generally governed by the chemical composition
372 of the hydrophobic phase (Freedman, 2017). A higher level of oxygenation in organic aerosol is
373 related with higher hydrophilicity, which would favor a homogeneous particle instead of phase
374 separation. Previous studies showed that LLPS did not occur for organic coating with O:C above
375 0.8 (You et al., 2013; You et al., 2014). The LLPS phenomenon in simple organic-inorganic
376 mixtures can also be affected by the functional groups. The maximum O:C for LLPS could be 0.71
377 for organics with multiple carboxylic and hydroxyl groups but low aromatic content (Song et al.,
378 2012) while the 2-butanone peroxide we used for both γ_{SO_2} measurement and prediction in the
379 present study has multiple peroxide groups with an O:C value of 0.75. Particle size could also have
380 impacts on phase separation (Cheng et al., 2015). Particle diameters in the current study are mainly
381 under 200 nm while a previous study showed particles smaller than this size are less likely to
382 experience LLPS (Veghte et al., 2013). We therefore believe that LLPS is not likely to be
383 responsible for the enhanced uptake rate observed under these experimental conditions.

384 Another explanation is the high solute strength in the concentrated aerosol phase. Although the
 385 aerosol water content for ammonium sulfate aerosol was found to be higher than that of malonic
 386 acid aerosol under RH 50%. As indicated in Fig. 4 and Fig. S8, the difference between the
 387 measured and predicted γ_{SO_2} is larger for ammonium sulfate aerosol than for malonic acid.
 388 Meanwhile, the calculated ionic strength in aerosol liquid phase under RH 50% for ammonium
 389 sulfate (40 mol kg^{-1}) is significantly larger than that of malonic acid (0.45 mol kg^{-1}). It has been
 390 previously reported that the reaction rate between sulfite and hydrogen peroxide in aqueous phase
 391 increases with ionic strength (Maaß et al., 1999). Based on the reaction mechanisms proposed for
 392 dissolved SO_2 and hydrogen peroxide (Halperin and Taube, 1952), we speculate the reaction



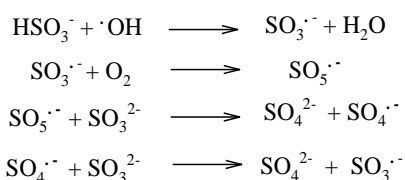
393 between aqueous phase S(IV) and organic peroxides to follow a similar mechanism:



394
 395 where the overall rate constant is equal to $k \frac{K}{K_a}$, assuming fast equilibrium steps for reactions 6 and
 396 7. Dissociated solutes are surrounded by an extended solvation shell which could affect the
 397 reaction rates (Herrmann, 2003). Fewer available free water molecules would therefore shift the

398 equilibrium to the right in equation (6). Additionally, higher ionic strength also corresponds to an
 399 increased concentration of electrolytes in the aqueous phase, which could hinder the dissociation
 400 of the peroxymonosulfurous acid and shift the equilibrium in equation (7) to the right. In recent
 401 work by Liu et al. (2020), the rate of S(IV) oxidation by H₂O₂ can be enhanced by up to a factor
 402 of 50 in aerosol aqueous phase compared to that of dilute solution. The highest ionic strength at
 403 which such enhancement was measured for the H₂O₂ oxidation pathway was 15 mol kg⁻¹ (Liu et
 404 al., 2020).

405 Whereas the above analysis is based on the assumption that all the chemistry occurs in the bulk
 406 component of the particle, it is also possible that some component of the reaction occurs at the gas-
 407 particle interface and the overall kinetics can be affected by interfacial characteristics. For example,
 408 an enhanced ionic strength in the aerosol phase can also impact the interfacial reaction mechanisms.
 409 Previous study has shown evidence that interfacial chemistry is important for SO₂ oxidation in the
 410 aerosol phase (Laskin et al., 2003). With higher ionic strength, anions partitioning to the air-liquid
 411 interface can promote the overall reaction kinetics via proton transfer and thus accelerate the
 412 interfacial chemistry (Knipping et al., 2000; Mishra et al., 2012; Mekic et al., 2018; Mekic et al.,
 413 2020; Wei et al., 2018; Ruiz-Lopez et al., 2020). In addition to the catalytic effects of protons
 414 indicated in Eqn.6-8, Hung et al. (2015, 2018) observed significant SO₃^{·-} signal at the acidic
 415 microdroplet surface, which can promote sulfate formation via radical propagation chain initiated
 416 by surrounding radicals and molecular oxygen (Eqn. 9-12):



(9) Formatted: Not Highlight

(10) Formatted: Subscript

(11) Formatted: Font: Bold, Superscript

(12) Formatted: Superscript

(9) Formatted: Font: 12 pt

(10) Formatted: Font: 12 pt

(11) Formatted: Font: 12 pt

(12) Formatted: Font: 12 pt

(9) Formatted: Font: 12 pt

(10) Formatted: Font: 12 pt

(11) Formatted: Font: 12 pt

(12) Formatted: Font: 12 pt

418 where the hydroxy radical can potentially be produced from decomposition of the labile organic
419 peroxide in our system (Tong et al., 2016). However, we cannot distinguish whether the interfacial
420 protons promote sulfate formation by catalyze the peroxide S(IV) oxidation pathway or the sulfur
421 radical pathway at the current stage. In the recent study by Wei et al. (2018), a pH gradient was
422 observed for phosphate-buffered aerosol droplets with the proton accumulated at the interface.
423 Base on the pH-dependent aqueous phase kinetics measured in our previous work (Wang et al.,
424 2019), such interfacial proton accumulation could potentially explain the enhanced kinetics we
425 observed for aerosol in the current study. However, the chemical compositions are quite different.
426 While phosphate-buffered particles were studied in Wei et al. (2018), acidic ammonium sulfate
427 aerosol was used in our study. Also, the particle size in Wei et al. (2018) is significantly larger (20
428 µm) than what was studied in the current study (200 nm). However, it Thus, it should be noted that
429 there is no direct evidence from the current study showing the direct relationship between the
430 interfacial properties and γ_{SO_2} , and future studies are warranted.

Formatted: Not Highlight

431 Therefore, while more studies are needed to clearly delineate the roles of ionic strength, interfacial
432 activity, bulk reactivity, and particle phase state quantitatively, the enhancement of SO₂ oxidation
433 kinetics by highly concentrated aerosol particles compared to dilute aqueous solutions are
434 concluded to be large (factor of 15-50) for the experimental conditions in the current study.

435

436 **3.4 SO₂ uptake and aerosol pH**

437 As indicated by the proposed reaction mechanisms (Eqn. 6-8), protons are important reaction
438 intermediates for this SO₂ oxidation pathway. Previously, the aqueous phase reaction rate
439 constants between organic peroxides and dissolved SO₂ were measured to be pH dependent
440 (Wang et al., 2019). Moreover, the dissolution equilibrium of SO₂ into aqueous phase is also pH

441 sensitive (Seinfeld and Pandis, 2012). Besides, many studies have shown that the uptake kinetics
442 for gaseous species can be affected by the condensed phase pH (Shi et al., 1999; Gaston et al.,
443 2014; Drozd et al., 2013; Jang and Kamens, 2001; Liu et al., 2015). Reactive uptake of ammonia
444 was observed to depend on condensed phase acidity (Shi et al., 1999). Heterogeneous
445 condensation of isoprene-derived epoxydiol onto seed aerosol was found to increase with proton
446 concentration (Gaston et al., 2014). In the current study, the potential impact from particle phase
447 pH on γ_{SO_2} was explored by adding HCl into the atomizing solution. To estimate the particle
448 phase pH, two different methods associated with two different assumptions were used. In the
449 first scenario, the aerosol pH in each experiment was estimated using the E-AIM III model
450 (Clegg et al., 1998) based on the initial molar ratios of inorganic species (H^+ , NH_4^+ , SO_4^{2-} , Cl^-) in
451 the atomizing solution and measured RH (around 50%). In the second scenario, the additional
452 sulfate formed from reactive uptake of SO_2 was taken into consideration. The partitioning of HCl
453 was allowed in the model simulation for both scenarios. The formation of sulfate would enhance
454 the proton concentration in the aerosol liquid phase thus lower the aerosol pH. The average pH
455 during the SO_2 uptake process is likely in between these two extremes.

456 Fig. 5 shows the measured reactive uptake coefficients of SO_2 as a function of the calculated pH.

457 The reactive uptake coefficient was found to weakly increase with ~~increasing proton~~
458 ~~concentrations decreasing pH (decreasing pH)~~, which is consistent with acid-catalyzed reactions
459 between peroxides and dissolved SO_2 as measured in the bulk phase (Lind et al., 1987; Wang et
460 al., 2019). γ_{SO_2} was also predicted for the same range of pH based on Eqn. 5 and the pH-
461 dependent bulk-phase reaction rate constants measured previously (Wang et al., 2019). Indicated
462 by Fig. 5, the measured γ_{SO_2} again exceeds the predicted γ_{SO_2} by about a factor of 50, which is
463 consistent with what we reported earlier and is likely due to the effects of aerosol ionic strength.

464 Unlike the observed γ_{SO_2} , however, the predicted γ_{SO_2} does not exhibit a monotonic trend. γ_{SO_2} is
465 expected to decrease with decreasing pH at high pH (>2) as the effective Henry's law constant of
466 SO_2 decreases with higher acidity (Seinfeld and Pandis, 2012). γ_{SO_2} is not expected to increase
467 with decreasing pH until pH is below 2 where the acidity enhancement in reaction rate constant
468 exceeds the decrease in SO_2 solubility. As illustrated earlier, extrapolating dilute aqueous-phase
469 kinetics to the highly concentrated aerosol requires considering effects from high solute strength.
470 Solute strength may change the pH dependence of γ_{SO_2} in two ways. First, the solubility of SO_2
471 may decrease and become less dependent on pH as ionic strength increases (Rodríguez-Sevilla et
472 al., 2002). A former study (Leng et al., 2015) has shown that the effective Henry's law of
473 triethylamine decreases with increased ionic strength. Another potential explanation is that the
474 aqueous phase reaction rate constant can be more pH-dependent at high ionic strengths than what
475 we measured previously in dilute solutions. In either case, the inflection of the predicted γ_{SO_2}
476 would change and γ_{SO_2} could become more negatively dependent on pH ($d[\gamma_{\text{SO}_2}]/d[\text{pH}]$ becomes
477 less positive in the high pH range and/or more negative in the low pH range), which would
478 match more closely with the observed dependence. It should also be noted that there are
479 substantial uncertainties in estimating pH values, originating from the partitioning of organics,
480 organic-inorganic phase separations, mixing state of specific ions, uncertain activity coefficients
481 and the propagation of RH uncertainties (Clegg et al., 2008; Fountoukis et al., 2009; Guo et al.,
482 2016). ~~since~~ Also, the reactive uptake is a dynamic process and will influence aerosol pH in turn
483 upon sulfate formation. In summary, while the magnitude of predicted γ_{SO_2} is consistent with our
484 expected values (after accounting for the enhancement by high aerosol solute strength), we
485 cannot fully explain the dependence of γ_{SO_2} on aerosol pH at the current stage. Future studies
486 should investigate how the effective Henry's law of SO_2 and pH dependence of reaction rate

487 constants vary in aerosol liquid phase with high solute strength in order to have a more
488 comprehensive understanding of the relationship between γ_{SO_2} and aerosol pH.

489 **3.4 SO₂ uptake onto SOA**

490 γ_{SO_2} was measured for a few model SOA systems, as organic peroxides are abundant in SOA
491 (Surratt et al., 2006;Kautzman et al., 2009;Krapf et al., 2016;Bonn et al., 2004). Here we studied
492 SOA formed from monoterpene ozonolysis and toluene photooxidation. It should be noted that
493 for the γ_{SO_2} measurements of toluene SOA, a strong hydrocarbon interference was observed with
494 the SO₂ analyzer, likely stemming from the high concentrations of gas-phase aromatic
495 compounds. A rough estimate of the uptake rate for toluene SOA from aerosol mass
496 spectrometer sulfate measurements is provided in the SI (Section 1). The reactive uptake
497 coefficient of SO₂ onto Saharan mineral dust was reported on the order of 10^{-5} (Adams et al.,
498 2005). γ_{SO_2} onto dust with the coexistence of NO₂ and NH₃ under various RH conditions were
499 measured to be 10^{-7} to 10^{-5} (Zhang et al., 2019). For a variety of metal oxides, SO₂ reactive
500 uptake coefficients were quantified to be between 10^{-6} and 10^{-4} (Usher et al., 2002; Fu et al.,
501 2007; Shang et al., 2010). More recently, γ_{SO_2} studied for heterogeneous sulfate formation by
502 photolysis of particulate nitrate were reported in the range of 10^{-6} to 10^{-5} (Gen et al., 2019). As
503 shown in Fig. 6, γ_{SO_2} for all SOA systems were measured to be on the order of 10^{-4} . Similar γ_{SO_2}
504 values on the order of 10^{-4} were measured for α -pinene SOA by Yao et al. (2019), and 10^{-5} for
505 limonene SOA estimated from the chamber study by Ye et al. (2018). The reaction products
506 from this SOA and SO₂ interaction will be reported in a separate study.

507

508 **4. Atmospheric Implications**

509 Oxidation of atmospheric hydrocarbons produces reactive intermediates that can potentially
510 interact with SO₂ and form particulate sulfate, contributing to PM formation and growth (Berndt
511 et al., 2015;Mauldin et al., 2012;Yao et al., 2019). Organic peroxides generated from both
512 biogenic and anthropogenic hydrocarbon emissions are abundant in submicron aerosol. Given
513 that they are highly reactive with relatively short lifetimes (Bonn et al., 2004;Krapf et al.,
514 2016;Qiu et al., 2020), these species could serve as important condensed phase oxidants for gas
515 phase SO₂. Combining laboratory measurements and model predictions, the current study
516 investigated heterogeneous reactions between SO₂ and particulate organic peroxide. The
517 measured γ_{SO_2} for organic peroxide containing aerosol ranges from 10⁻⁵ to 10⁻² in this study.
518 Based on the modeling work by Wang et al. (2014), adding an SO₂ uptake pathway to GEOS-
519 Chem with a reactive uptake coefficient of 10⁻⁴ could improve the surface sulfate prediction by
520 more than 50% during a severe haze episode over North China (RH 50%), suggesting the
521 potential importance of this multiphase reaction pathway, especially when SOA is the dominant
522 component in particulate matter.

523 The dependence of the heterogeneous kinetics on RH, aerosol pH, peroxide type, and peroxide
524 content were also evaluated. The experimentally measured γ_{SO_2} was found to be consistently
525 higher than that predicted from reaction kinetics with organic peroxides in the dilute aqueous
526 phase. This discrepancy can be potentially explained by the effects of high ionic strength
527 presented in the aerosol, suggesting that the impact from highly concentrated solutes needs to be
528 taken into consideration when applying aqueous phase kinetics to aerosol multiphase chemistry,
529 especially for particles containing strong electrolytes. We also observed that the kinetics of this
530 multiphase reaction exhibit a weak dependence on pH. Increasing the condensed-phase acidity
531 may enhances the heterogeneous rate constant at low pH-range, and while this pH dependence is

532 consistent with that of the aqueous phase reaction rate constant measured previously, it is not
533 consistent with the decrease of effective Henry's law constant of SO₂ along with enhanced
534 acidity. Also, it is likely that within the uncertainties, there may not be an observable γ_{SO_2} -pH
535 trend. Currently, we are not able to fully explain the pH dependence, ~~likely due to the~~
536 ~~uncertainties from high ionic strength,~~ and further studies are warranted. Particle phase peroxide
537 content was observed to be linearly correlated with γ_{SO_2} . Moreover, γ_{SO_2} measured for 2-butanone
538 peroxide was found to be orders of magnitude higher than that of cumene hydroperoxide and
539 tert-butyl hydroperoxide. The difference in γ_{SO_2} among various types of organic peroxides can be
540 partially explained by their condensed-phase reactivity and gas-particle partitioning.

541 In general, we found the observed γ_{SO_2} in this study can be summarized using the following
542 semiempirical multilinear relationship:

$$543 \quad \log \gamma = -1.7 + 0.0024 \times k'' + 0.46 \times PAS + 0.024 \times RH - 1.9 \times Vp \quad (13)$$

544 where γ is the reactive uptake coefficient, k'' is the aqueous phase S(IV) oxidation rate constant
545 ($\text{M}^{-1} \text{s}^{-1}$), PAS is the molar ratio between particulate peroxide and ammonium sulfate in the
546 atomizing solution, which is a proxy for the amount of peroxide in both gas and particle phases
547 applied in the current study, RH is the relative humidity (%), Vp is the vapour pressure (kPa) of
548 the peroxide. Fig. 7 illustrates the degree to which this semi-empirical expression describes the
549 experimental data for ammonium sulfate aerosol mixed with the three types of organic peroxides.
550 Residual evaluations of this multilinear regression can be found Fig. S9. We caution that this
551 equation is not directly applicable to atmospheric models in its current form, especially since the
552 particle phase peroxide content (PAS) value we applied as input is a calculated value, rather than
553 a measurement. However, it illustrates the internal consistency of our experimental results across
554 a range of RH , peroxide content, and aqueous phase reactivities, which are the key variables for

555 uptake rates. Better understanding of ionic strengths and pH in aerosol, either through modeling
556 or direct measurements of these variables, is needed to establish the coefficient dependence.
557 Future studies should be focused on exploring γ_{SO_2} and the reaction products for various types of
558 SOA as well as ambient particles under atmospherically relevant conditions, evaluating the
559 underlying impacts from photochemical condition, chemical composition, particle morphology,
560 ionic strength and interfacial properties on this multiphase physicochemical process. Overall,
561 γ_{SO_2} presented in our study and its relationship with ambient RH, aerosol pH, ionic strength,
562 particulate peroxide content and type could provide a framework for the implementation of this
563 heterogeneous mechanism in atmospheric models to have a better understanding of ambient
564 sulfate formation and particle growth.

565

566

567

568

569

570

571

572

573

574

575

576

577

578 *Author contributions*

579 A.W.H. C. and S.W. designed the study. S.W., T. L., and J. J. performed the experiments. S.W.,
580 A.W.H. C., T. L., and J. J. analyzed data. S.W. and A.W.H. C. wrote the manuscript with the
581 input from all co-authors.

582

583 *Data availability*

584 All data presented in this study are available in the supplemental material and have been
585 deposited in figshare.

586

587 *Associated content*

588 Supporting Information.

589

590 *Competing interests*

591 The authors declare no competing financial interest.

592

593 *Acknowledgements*

594 This work was supported by Natural Sciences and Engineering Research Council Discovery Grant.

595 The authors would like to thank Dr. Greg Evans, Dr. Yue Zhao and Dr. Christopher Lim for helpful
596 comments and discussions. Special thanks to SOCAAR for providing the SO₂ analyzer.

597

598

599

600

601

602 **Reference**

- 603 Abbatt, J. P. D., Lee, A. K. Y., and Thornton, J. A.: Quantifying trace gas uptake to tropospheric
604 aerosol: recent advances and remaining challenges, *Chem. Soc. Rev.*, 41, 6555–6581,
605 <https://doi.org/10.1039/c2cs35052a>, 2012.
- 606 Adams, J. W., Rodriguez, D., and Cox, R. A.: The uptake of SO₂ on Saharan dust: a flow tube
607 study, *Atmos. Chem. Phys.*, 5, 2643–2676, doi:10.5194/acp-5-2643-2005, 2005.
- 608 Andreae, M.O., Afchine, A., Albrecht, R., Holanda, B.A., Artaxo, P., Barbosa, H.M., Borrmann,
609 S., Cecchini, M.A., Costa, A., Dollner, M. and Fütterer, D.: Aerosol characteristics and particle
610 production in the upper troposphere over the Amazon Basin, *Atmos. Chem. Phys.*, 18, 921–961,
611 2018.
- 612 Atkinson, R., and Arey, J.: Atmospheric degradation of volatile organic compounds, *Chem.*
613 *Rev.*, 103, 4605-4638, 2003.
- 614 Berndt, T., Richters, S., Kaethner, R., Voigtländer, J., Stratmann, F., Sipilä, M., Kulmala, M.,
615 and Herrmann, H.: Gas-phase ozonolysis of cycloalkenes: Formation of highly oxidized RO₂
616 radicals and their reactions with NO, NO₂, SO₂, and other RO₂ radicals, *J. Phys. Chem. A*, 119,
617 10336-10348, 10.1021/acs.jpca.5b07295, 2015.
- 618 Bianchi, F., Kurtén, T., Riva, M., Mohr, C., Rissanen, M. P., Roldin, P., Berndt, T., Crouse, J.
619 D., Wennberg, P. O., Mentel, T. F., Wildt, J., Junninen, H., Jokinen, T., Kulmala, M., Worsnop,
620 D. R., Thornton, J. A., Donahue, N., Kjaergaard, H. G., and Ehn, M.: Highly oxygenated organic
621 molecules (HOM) from gas-phase autoxidation involving peroxy radicals: A key contributor to
622 atmospheric aerosol, *Chem. Rev.*, 119, 3472-3509, 10.1021/acs.chemrev.8b00395, 2019.
- 623 Bonn, B., von Kuhlmann, R., and Lawrence, M. G.: High contribution of biogenic
624 hydroperoxides to secondary organic aerosol formation, *Geophys. Res. Lett.*, 31, L10108,
625 <https://doi.org/10.1029/2003GL019172>, 2004.
- 626 Chen, Q., Farmer, D. K., Schneider, J., Zorn, S. R., Heald, C. L., Karl, T. G., Guenther, A.,
627 Allan, J. D., Robinson, N., Coe, H., Kimmel, J. R., Pauliquevis, T., Borrmann, S., Pöschl, U.,
628 Andreae, M. O., Artaxo, P., Jimenez, J. L., and Martin, S. T.: Mass spectral characterization of
629 submicron biogenic organic particles in the Amazon Basin, *Geophys. Res. Lett.*, 36, L20806,
630 <https://doi.org/10.1029/2009GL039880>, 2009.
- 631 Chen, T., Chu, B., Ge, Y., Zhang, S., Ma, Q., He, H., and Li, S.-M.: Enhancement of aqueous
632 sulfate formation by the coexistence of NO₂/NH₃ under high ionic strengths in aerosol water,
633 *Environ. Pollut.*, 252, 236-244, <https://doi.org/10.1016/j.envpol.2019.05.119>, 2019.
- 634 Cheng, Y., Su, H., Koop, T., Mikhailov, E., and Pöschl, U.: Size dependence of phase transitions
635 in aerosol nanoparticles, *Nat. Commun.*, 6, 5923, 10.1038/ncomms6923, 2015.
- 636 Cheng, Y. F., Zheng, G. J., Wei, C., Mu, Q., Zheng, B., Wang, Z. B., Gao, M., Zhang, Q., He, K.
637 B., Carmichael, G., Pöschl, U., and Su, H.: Reactive nitrogen chemistry in aerosol water as a
638 source of sulfate during haze events in China, *Sci. Adv.*, 2, e1601530, 2016.
- 639 Ciobanu, V. G., Marcolli, C., Krieger, U. K., Weers, U., and Peter, T.: Liquid-liquid phase
640 separation in mixed organic/inorganic aerosol particles, *J. Phys. Chem. A*, 113, 10966–10978,
641 2009.

642 Clegg, S. L., Brimblecombe, P., and Wexler, A. S.: Thermodynamic model of the system
643 $\text{H}^+ - \text{NH}_4^+ - \text{Na}^+ - \text{SO}_4^{2-} - \text{NO}_3^- - \text{Cl}^- - \text{H}_2\text{O}$ at 298.15 K, *J. Phys. Chem. A*, 102, 2155–2171,
644 <https://doi.org/10.1021/jp973043j>, 1998.

645 [Clegg, S. L., Kleeman, M. J., Griffin, R. J., and Seinfeld, J. H.: Effects of uncertainties in the](#)
646 [thermodynamic properties of aerosol components in an air quality model – Part 1: Treatment of](#)
647 [inorganic electrolytes and organic compounds in the condensed phase, *Atmos. Chem. Phys.*, 8,](#)
648 [1057–1085, <http://www.atmos-chem-phys.net/8/1057/2008/>, 2008.](#)

649 [Ding, J., Zhao, P., Su, J., Dong, Q., Du, X., and Zhang, Y.: Aerosol pH and its driving factors in](#)
650 [Beijing, *Atmos. Chem. Phys.*, 19, 7939–7954, 10.5194/acp-19-7939-2019, 2019.](#)

651 Docherty, K. S., Wu, W., Lim, Y. B., and Ziemann, P. J.: Contributions of organic peroxides to
652 secondary aerosol formed from reactions of monoterpenes with O_3 , *Environ. Sci. Technol.*, 39,
653 4049–4059, 2005.

654 Dovrou, E., Rivera-Rios, J. C., Bates, K. H., and Keutsch, F. N.: Sulfate formation via cloud
655 processing from isoprene hydroxyl hydroperoxides (ISOPOOH), *Environ. Sci. Technol.*, 53,
656 12476–12484, 10.1021/acs.est.9b04645, 2019.

657 Drozd, G. T., Woo, J. L., and McNeill, V. F.: Self-limited uptake of α -pinene oxide to acidic
658 aerosol: the effects of liquid-liquid phase separation and implications for the formation of
659 secondary organic aerosol and organosulfates from epoxides, *Atmos. Chem. Phys.*, 13, 8255–
660 8263, doi:10.5194/acp-13-8255-2013, 2013.

661 Epstein, S. A., Blair, S. L., and Nizkorodov, S. A.: Direct photolysis of α -pinene ozonolysis
662 secondary organic aerosol: effect on particle mass and peroxide content, *Environ. Sci. Technol.*,
663 48, 11251–11258, 2014.

664 Fairlie, T. D., Jacob, D. J., Dibb, J. E., Alexander, B., Avery, M. A., van Donkelaar, A., and
665 Zhang, L.: Impact of mineral dust on nitrate, sulfate, and ozone in transpacific Asian pollution
666 plumes, *Atmos. Chem. Phys.*, 10, 3999–4012, doi:10.5194/acp-10-3999-2010, 2010.

667 [Fountoukis, C., Nenes, A., Sullivan, A., Weber, R., Van Reken, T., Fischer, M., Matas, E.,](#)
668 [Moya, M., Farmer, D., and Cohen, R. C.: Thermodynamic characterization of Mexico City](#)
669 [aerosol during MILAGRO 2006, *Atmos. Chem. Phys.*, 9, 2141–2156, 2009.](#)

670 Freedman, M. A.: Phase separation in organic aerosol, *Chem. Soc. Rev.*, 46, 7694–7705,
671 <https://doi.org/10.1039/C6CS00783J>, 2017.

672 Fu, H. B., Wang, X., Wu, H. B., Yin, Y., and Chen, J. M.: Heterogeneous uptake and oxidation
673 of SO_2 on iron oxides, *J. Phys. Chem. C*, 111, 6077–6085, 2007.

674 Gao, M., Carmichael, G. R., Wang, Y., Saide, P. E., Yu, M., Xin, J., Liu, Z., and Wang, Z.:
675 Modeling study of the 2010 regional haze event in the North China Plain, *Atmos. Chem. Phys.*,
676 16, 1673–1691, <https://doi.org/10.5194/acp-16-1673-2016>, 2016.

677 Gaston, C. J., Riedel, T. P., Zhang, Z., Gold, A., Surratt, J. D., and Thornton, J. A.: Reactive
678 uptake of an isoprene-derived epoxydiol to submicron aerosol particles, *Environ. Sci. Technol.*,
679 48, 11178–11186, 10.1021/es5034266, 2014.

680 Gen, M., Zhang, R., Huang, D. D., Li, Y., and Chan, C. K.: Heterogeneous SO_2 oxidation in
681 sulfate formation by photolysis of particulate nitrate, *Environ. Sci. Tech. Lett.*, 6, 86–91,
682 <https://doi.org/10.1021/acs.estlett.8b00681>, 2019.

Formatted: Default Paragraph Font, Font color: Text 1

683 Griffiths, P. T., Badger, C. L., Cox, R. A., Folkers, M., Henk, H. H., and Mentel, T. F.: Reactive
684 uptake of N₂O₅ by aerosols containing dicarboxylic acids. Effect of particle phase, composition,
685 and nitrate content, *J. Phys. Chem. A*, 113, 5082-5090, 10.1021/jp8096814, 2009.

686 Gunz, D. W. and Hoffmann, M. R.: Atmospheric chemistry of peroxides: A review, *Atmos.*
687 *Environ.*, 24A, 1601–1633, [https://doi.org/10.1016/0960-1686\(90\)90496-A](https://doi.org/10.1016/0960-1686(90)90496-A), 1990.

688 [Guo, H., Sullivan, A. P., Campuzano-Jost, P., Schroder, J. C., LopezHilfiker, F. D., Dibb, J. E.,](#)
689 [Jimenez, J. L., Thornton, J. A., Brown, S. S., Nenes, A., and Weber, R. J.: Fine particle pH and](#)
690 [the partitioning of nitric acid during winter in the northeastern United States, *J. Geophys. Res.*](#)
691 [Atmos., 121, 10355–10376, <https://doi.org/10.1002/2016JD025311>, 2016.](#)

692 Guo, H., Weber, R. J., and Nenes, A.: High levels of ammonia do not raise fine particle pH
693 sufficiently to yield nitrogen oxide-dominated sulfate production, *Sci. Rep.*, 7, 12109, 2017.

694 Hallquist, M., Wenger, J. C., Baltensperger, U., Rudich, Y., Simpson, D., Claeys, M., Dommen,
695 J., Donahue, N. M., George, C., Goldstein, A. H., Hamilton, J. F., Herrmann, H., Hoffmann, T.,
696 Iinuma, Y., Jang, M., Jenkin, M. E., Jimenez, J. L., Kiendler-Scharr, A., Maenhaut, W.,
697 McFiggans, G., Mentel, Th. F., Monod, A., Prévôt, A. S. H., Seinfeld, J. H., Surratt, J. D.,
698 Szmigielski, R., and Wildt, J.: The formation, properties and impact of secondary organic
699 aerosol: current and emerging issues, *Atmos. Chem. Phys.*, 9, 5155–5236, 2009.

700 Halperin, J., and Taube, H.: The transfer of oxygen atoms in oxidation—reduction reactions. IV.
701 The reaction of hydrogen peroxide with sulfite and thiosulfate, and of oxygen, manganese
702 dioxide and of permanganate with sulfite, *J. Am. Chem. Soc.*, 74, 380-382, 1952.

703 Hanson, D. R., Ravishankara, A. R., and Solomon, S.: Heterogeneous reactions in sulfuric acid
704 aerosols: A framework for model calculations, *J. Geophys. Res.*, 99, 3615, [https://doi.org/](https://doi.org/10.1029/93JD02932)
705 [10.1029/93JD02932](https://doi.org/10.1029/93JD02932), 1994.

706 Hartz, K. E. H., Rosenorn, T., Ferchak, S. R., Raymond, T. M., Bilde, M., Donahue, N. M., and
707 Pandis, S. N.: Cloud condensation nuclei activation of monoterpene and sesquiterpene
708 secondary organic aerosol, *J. Geophys. Res.-Atmos.*, 110(D14), D14208, 2005.

709 He, L.-Y., Huang, X.-F., Xue, L., Hu, M., Lin, Y., Zheng, J., Zhang, R., and Zhang, Y.-H.:
710 Submicron aerosol analysis and organic source apportionment in an urban atmosphere
711 in Pearl River Delta of China using high-resolution aerosol mass spectrometry, *J. Geophys. Res.*
712 *Atmos.*, 116, D12304, <https://doi.org/10.1029/2010JD014566>, 2011.

713 Herrmann, H.: Kinetics of aqueous phase reactions relevant for atmospheric chemistry, *Chem.*
714 *Rev.*, 103, 4691–4716, 2003.

715 Hildebrandt, L., Donahue, N. M., Pandis, S. N.: High formation of secondary organic aerosol
716 from the photo-oxidation of toluene, *Atmos. Chem. Phys.*, 9, 2973–2986, 2009.

717 Huang, L., An, J., Koo, B., Yarwood, G., Yan, R., Wang, Y., Huang, C., and Li, L.: Sulfate
718 formation during heavy winter haze events and the potential contribution from heterogeneous
719 SO₂ + NO₂ reactions in the Yangtze River Delta region, China, *Atmos. Chem. Phys.*, 19, 14311-
720 14328, 10.5194/acp-19-14311-2019, 2019.

721 Huang, L., Coddens, E. M., and Grassian, V. H.: Formation of organosulfur compounds from
722 aqueous phase reactions of S (IV) with methacrolein and methyl vinyl ketone in the presence of
723 transition metal ions, *ACS Earth Space Chem.*, 3, 1749-1755, 2019.

724 Huang, L., Liu, T. and Grassian, V. H.: Radical-initiated formation of aromatic organosulfates
725 and sulfonates in the aqueous phase. *Environ. Sci. Technol.*, 54, 11857–11864, 2020.

726 Huang, R. J., Zhang, Y. L., Bozzetti, C., Ho, K. F., Cao, J. J., Han, Y. M., Daellenbach, K. R.,
727 Slowik, J. G., Platt, S. M., Canonaco, F., Zotter, P., Wolf, R., Pieber, S. M., Bruns, E. A., Crippa,
728 M., Ciarelli, G., Piazzalunga, A., Schwikowski, M., Abbaszade, G., Schnelle-Kreis, J.,
729 Zimmermann, R., An, Z., Szidat, S., Baltensperger, U., Haddad, I. E., and Prevot, A. S. H.: High
730 secondary aerosol contribution to particulate pollution during haze events in China, *Nature*, 514,
731 218–222, 2014.

732 Huang, R. J., He, Y., Duan, J., Li, Y., Chen, Q., Zheng, Y., Chen, Y., Hu, W., Lin, C., Ni, H.,
733 Dai, W., Cao, J., Wu, Y., Zhang, R., Xu, W., Ovadnevaite, J., Ceburnis, D., Hoffmann, T., and
734 O'Dowd, C. D.: Contrasting sources and processes of particulate species in haze days with low
735 and high relative humidity in wintertime Beijing, *Atmos. Chem. Phys.*, 20, 9101-9114,
736 10.5194/acp-20-9101-2020, 2020.

737 [Hung, H. M. and Hoffmann, M. R.: Oxidation of gas-phase SO₂ on the surfaces of acidic
738 microdroplets: Implications for sulfate and sulfate radical anion formation in the atmospheric
739 liquid phase. *Environ. Sci. Technol.*, 49, 13768–13776, 2015.](#)

740 [Hung, H. M., Hsu, M. N., and Hoffmann, M. R.: Quantification of SO₂ oxidation on interfacial
741 surfaces of acidic micro-droplets: Implication for ambient sulfate formation. *Environ. Sci.
742 Technol.*, 52, 9079–9086. <https://doi.org/10.1021/acs.est.8b01391>, 2018.](#)

743 Jang, M., and Kamens, R. M.: Atmospheric secondary aerosol formation by heterogeneous
744 reactions of aldehydes in the presence of a sulfuric acid aerosol catalyst, *Environ. Sci. Technol.*,
745 35, 4758-4766, 10.1021/es010790s, 2001.

746 Jimenez, J. L., Canagaratna, M. R., Donahue, N. M., Prevot, A. S. H., Zhang, Q., Kroll, J. H.,
747 DeCarlo, P. F., Allan, J. D., Coe, H., Ng, N. L., Aiken, A. C., Docherty, K. S., Ulbrich, I. M.,
748 Grieshop, A. P., Robinson, A. L., Duplissy, J., Smith, J. D., Wilson, K. R., Lanz, V. A., Hueglin,
749 C., Sun, Y. L., Tian, J., Laaksonen, A., Raatikainen, T., Rautiainen, J., Vaattovaara, P., Ehn, M.,
750 Kulmala, M., Tomlinson, J. M., Collins, D. R., Cubison, M. J., Dunlea, J., Huffman, J. A.,
751 Onasch, T. B., Alfarra, M. R., Williams, P. I., Bower, K., Kondo, Y., Schneider, J., Drewnick,
752 F., Borrmann, S., Weimer, S., Demerjian, K., Salcedo, D., Cottrell, L., Griffin, R., Takami, A.,
753 Miyoshi, T., Hatakeyama, S., Shimojo, A., Sun, J. Y., Zhang, Y. M., Dzepina, K., Kimmel,
754 J. R., Sueper, D., Jayne, J. T., Herndon, S. C., Trimborn, A. M., Williams, L. R., Wood, E. C.,
755 Middlebrook, A. M., Kolb, C. E., Baltensperger, U., and Worsnop, D. R.: Evolution of organic
756 aerosols in the atmosphere, *Science*, 326, 1525–1529, <https://doi.org/10.1126/science.1180353>,
757 2009.

758 Kautzman, K., Surratt, J., Chan, M., Chan, A., Hersey, S., Chhabra, P., Dalleska, N., Wennberg,
759 P., Flagan, R., and Seinfeld, J.: Chemical composition of gas-and aerosol-phase products from
760 the photooxidation of naphthalene, *J. Phys. Chem. A*, 114, 913-934, 2009.

761 Knipping, E. M., Lakin, M. J., Foster, K. L., Jungwirth, P., Tobias, D. J., Gerber, R. B., Dabdub,
762 D., and Finlayson-Pitts, B. J.: Experiments and simulations of ion-enhanced interfacial chemistry
763 on aqueous NaCl aerosols, *Science*, 288, 301, 10.1126/science.288.5464.301, 2000.

764 Krapf, M., El Haddad, I., Bruns, E. A., Molteni, U., Daellenbach, K. R., Prévôt, A. S.,
765 Baltensperger, U., and Dommen, J.: Labile peroxides in secondary organic aerosol, *Chem*, 1,
766 603-616, 2016.

Formatted: Subscript

Formatted: Subscript

Formatted: Default Paragraph Font, Font: (Default)
Calibri, 11 pt, Font color: Text 1, Do not check spelling
or grammar

767 Laskin, A., Gaspar, D. J., Wang, W., Hunt, S. W., Cowin, J. P., Colson, S. D., and Finlayson-
768 Pitts, B. J.: Reactions at interfaces as a source of sulfate formation in sea-salt particles, *Science*,
769 301, 340, 10.1126/science.1085374, 2003.

770 Leng, C. B., Roberts, J. E., Zeng, G., Zhang, Y. H., and Liu, Y.: Effects of temperature, pH, and
771 ionic strength on the Henry's law constant of triethylamine, *Geophys. Res. Lett.*, 42, 3569-3575,
772 10.1002/2015gl063840, 2015.

773 Li, G., Bei, N., Cao, J., Huang, R., Wu, J., Feng, T., Wang, Y., Liu, S., Zhang, Q., Tie, X., and
774 Molina, L. T.: A possible pathway for rapid growth of sulfate during haze days in China, *Atmos.*
775 *Chem. Phys.*, 17, 3301–3316, <https://doi.org/10.5194/acp17-3301-2017>, 2017.

776 Li, J., Zhang, Y.L., Cao, F., Zhang, W., Fan, M., Lee, X., and Michalski, G.: Stable sulfur
777 isotopes revealed a major role of transition-metal ion-catalyzed SO₂ oxidation in haze episodes,
778 *Environ. Sci. Technol.*, 54, 2626–2634, <https://doi.org/10.1021/acs.est.9b07150>, 2020.

779 Lind, J. A., Lazrus, A. L., and Kok, G. L.: Aqueous phase oxidation of sulfur (IV) by hydrogen
780 peroxide, methylhydroperoxide, and peroxyacetic acid, *J. Geophys. Res. Atmos.*, 92, 4171-4177,
781 1987.

782 Liu, C., Chen, T., Liu, Y., Liu, J., He, H., Zhang, P.: Enhancement of secondary organic aerosol
783 formation and its oxidation state by SO₂ during photooxidation of 2-methoxyphenol, *Atmos.*
784 *Chem. Phys.*, 19, 2687-2700, 2019.

785 Liu, L., Bei, N., Wu, J., Liu, S., Zhou, J., Li, X., Yang, Q., Feng, T., Cao, J., Tie, X. and Li, G.:
786 Effects of stabilized Criegee intermediates (sCIs) on sulfate formation: a sensitivity analysis
787 during summertime in Beijing–Tianjin–Hebei (BTH), China, *Atmos. Chem. Phys.*, 19, 13341-
788 13354, 2019.

789 Liu, T., Clegg, S. L. and Abbatt, J. P. D.: Fast oxidation of sulfur dioxide by hydrogen peroxide
790 in deliquesced aerosol particles, *Proc. Natl. Acad. Sci. U. S. A.*, 117, 1354–1359, 2020.

791 Liu, Y., Liggio, J., Staebler, R., and Li, S. M.: Reactive uptake of ammonia to secondary organic
792 aerosols: kinetics of organonitrogen formation, *Atmos. Chem. Phys.*, 15, 13569–13584, 2015.

793 Maaß, F., Elias, H., and Wannowius, K. J.: Kinetics of the oxidation of hydrogen sulfite by
794 hydrogen peroxide in aqueous solution: ionic strength effects and temperature dependence,
795 *Atmos. Environ.*, 33, 4413-4419, [https://doi.org/10.1016/S1352-2310\(99\)00212-5](https://doi.org/10.1016/S1352-2310(99)00212-5), 1999.

796 Mauldin, R. L., Berndt, T., Sipilä, M., Paasonen, P., Petäjä, T., Kim, S., Kurtén, T., Stratmann,
797 F., Kerminen, V. M., and Kulmala, M.: A new atmospherically relevant oxidant of sulphur
798 dioxide, *Nature*, 488, 193–196, <https://doi.org/10.1038/nature11278>, 2012.

799 Mekic, M., Loisel, G., Zhou, W., Jiang, B., Vione, D., and Gligorovski, S.: Ionic-strength effects
800 on the reactive uptake of ozone on aqueous pyruvic acid: Implications for air–sea ozone
801 deposition, *Environ. Sci. Technol.*, 52, 12306-12315, 10.1021/acs.est.8b03196, 2018.

802 Mekic, M., Zeng, J., Zhou, W., Loisel, G., Jin, B., Li, X., Vione, D., and Gligorovski, S.: Ionic
803 strength effect on photochemistry of fluorene and dimethylsulfoxide at the air–sea interface:
804 Alternative formation pathway of organic sulfur compounds in a marine atmosphere, *ACS Earth*
805 *Space Chem.*, 4, 1029-1038, 10.1021/acsearthspacechem.0c00059, 2020.

806 Mishra, H., Enami, S., Nielsen, R. J., Hoffmann, M. R., Goddard, W. A., and Colussi, A. J.:
807 Anions dramatically enhance proton transfer through aqueous interfaces, *Proc. Natl. Acad. Sci.*
808 *U. S. A.*, 109, 10228-10232, 2012.

809 [Newland, M. J., Rickard, A. R., Vereecken, L., Muñoz, A., Ródenas, M., and Bloss, W. J.:](#)
810 [Atmospheric isoprene ozonolysis: impacts of stabilised Criegee intermediate reactions with SO₂,](#)
811 [H₂O and dimethyl sulfide, *Atmos. Chem. Phys.*, 15, 9521–9536, \[https://doi.org/10.5194/acp-15-\]\(https://doi.org/10.5194/acp-15-9521-2015\)](#)
812 [9521-2015, 2015.](#)

813 Ng, N., Kroll, J., Chan, A., Chhabra, P., Flagan, R., and Seinfeld, J.: Secondary organic aerosol
814 formation from m-xylene, toluene, and benzene, *Atmos. Chem. Phys.*, 7, 3909–3922,
815 <http://www.atmos-chem-phys.net/7/3909/2007/>, 2007.

816 Ng, N. L., Kwan, A. J., Surratt, J. D., Chan, A. W. H., Chhabra, P. S., Sorooshian, A., Pye, H. O.
817 T., Crouse, J. D., Wennberg, P. O., Flagan, R. C., and Seinfeld, J. H.: Secondary organic
818 aerosol (SOA) formation from reaction of isoprene with nitrate radicals (NO₃), *Atmos. Chem.*
819 *Phys.*, 8, 4117–4140, <http://www.atmos-chem-phys.net/8/4117/2008/>, 2008.

820 [Nguyen, T. B., Tyndall, G. S., Crouse, J. D., Teng, A. P., Bates, K. H., Schwantes, R. H.,](#)
821 [Coggon, M. M., Zhang, L., Feiner, P., Miller, D. O., Skog, K. M., Rivera-Rios, J. C., Dorris, M.,](#)
822 [Olson, K. F., Koss, A., Wild, R. J., Brown, S. S., Goldstein, A. H., de Gouw, J. A., Brune,](#)
823 [W. H., Keutsch, F. N., Seinfeld, J. H., and Wennberg, P. O.: Atmospheric fates of Criegee](#)
824 [intermediates in the ozonolysis of isoprene, *Phys. Chem. Chem. Phys.*, 18, 10 241–10 254,](#)
825 <https://doi.org/10.1039/C6CP00053C>, <http://dx.doi.org/10.1039/C6CP00053C>, 2016.

826 O'Brien, R. E., Wang, B., Kelly, S. T., Lundt, N., You, Y., Bertram, A. K., Leone, S. R., Laskin,
827 A., and Gilles, M. K.: Liquid–liquid phase separation in aerosol particles: Imaging at the
828 nanometer scale, *Environ. Sci. Technol.*, 49, 4995-5002, 10.1021/acs.est.5b00062, 2015.

829 Pankow, J. F. and Asher, W. E.: SIMPOL.1: a simple group contribution method for predicting
830 vapor pressures and enthalpies of vaporization of multifunctional organic compounds, *Atmos.*
831 *Chem. Phys.*, 8, 2773–2796, <http://www.atmos-chem-phys.net/8/2773/2008/>, 2008.

832 Qiu, J., Liang, Z., Tonokura, K., Colussi, A. J., and Enami, S.: Stability of monoterpene-derived
833 α -hydroxyalkyl-hydroperoxides in aqueous organic media – relevance to the fate of
834 hydroperoxides in aerosol particle phases, *Environ. Sci. Technol.*, 10.1021/acs.est.9b07497,
835 2020.

836 Rodríguez-Sevilla, J., Álvarez, M., Limiñana, G., Díaz, M. C.: Dilute SO₂ absorption equilibria
837 in aqueous HCl and NaCl solutions at 298.15 K, *J. Chem. Eng. Data*, 47, 1339-1345, 2002.

838 Ruiz-Lopez, M.F., Francisco, J.S., Martins-Costa, M.T. and Anglada, J.M.: Molecular reactions
839 at aqueous interfaces. *Nat. Rev. Chem.*, 1-17, 2020.

840 Seinfeld, J. H., and Pandis, S. N.: Atmospheric chemistry and physics: from air pollution to
841 climate change, John Wiley & Sons, 2012.

842 Sha, T., Ma, X., Jia, H., Tian, R., Chang, Y., Cao, F., and Zhang, Y.: Aerosol chemical
843 component: Simulations with WRF-Chem and comparison with observations in Nanjing, *Atmos.*
844 *Environ.*, 218, 116982, <https://doi.org/10.1016/j.atmosenv.2019.116982>, 2019.

845 Shang, J., Li, J., Zhu, T.: Heterogeneous reaction of SO₂ on TiO₂ particles. *Sci. China Chem.*, 53,
846 2637–2643, 2010.

Formatted: Subscript

Formatted: Subscript

847 [Shi, G., Xu, J., Peng, X., Xiao, Z., Chen, K., Tian, Y., Guan, X., Feng, Y., Yu, H., Nenes, A.,](#)
848 [and Russell, A. G.: pH of aerosols in a polluted atmosphere: Source contributions to highly](#)
849 [acidic aerosol, *Environ. Sci. Technol.*, 51, 4289-4296, 10.1021/acs.est.6b05736, 2017.](#)

850 Shi, Q., Davidovits, P., Jayne, J. T., Worsnop, D. R., and Kolb, C. E.: Uptake of gas-phase
851 ammonia. 1. Uptake by aqueous surfaces as a function of pH, *J. Phys. Chem. A*, 103, 8812-8823,
852 10.1021/jp991696p, 1999.

853 Song, M., Marcolli, C., Krieger, U. K., Zuend, A., and Peter, T.: Liquid-liquid phase separation
854 in aerosol particles: dependence on O:C, organic functionalities, and compositional complexity,
855 *Geophys. Res. Lett.*, 39, L19801, doi:10.1029/2012GL052807, 2012.

856 Song, S., Gao, M., Xu, W., Shao, J., Shi, G., Wang, S., Wang, Y., Sun, Y., and McElroy, M. B.:
857 Fine-particle pH for Beijing winter haze as inferred from different thermodynamic equilibrium
858 models, *Atmos. Chem. Phys.*, 18, 7423-7438, <https://doi.org/10.5194/acp-18-7423-2018>, 2018.

859 Song, S., Gao, M., Xu, W., Sun, Y., Worsnop, D. R., Jayne, J. T., Zhang, Y., Zhu, L., Li, M.,
860 Zhou, Z., Cheng, C., Lv, Y., Wang, Y., Peng, W., Xu, X., Lin, N., Wang, Y., Wang, S., Munger,
861 J. W., Jacob, D. J., and McElroy, M. B.: Possible heterogeneous chemistry of hydroxy
862 methanesulfonate (HMS) in northern China winter haze, *Atmos. Chem. Phys.*, 19, 1357-1371,
863 <https://doi.org/10.5194/acp-19-1357-2019>, 2019.

864 Su, H., Cheng, Y., and Pöschl, U.: New multiphase chemical processes influencing atmospheric
865 aerosols, air quality, and climate in the anthropocene, *Accounts Chem. Res.*, 53, 2034-2043,
866 <https://doi.org/10.1021/acs.accounts.0c00246>, 2020.

867 Sun, Y., Wang, Z., Fu, P., Jiang, Q., Yang, T., Li, J., and Ge, X.: The impact of relative humidity
868 on aerosol composition and evolution processes during wintertime in Beijing, China, *Atmos.*
869 *Environ.*, 77, 927-934, 2013.

870 Surratt, J. D., Murphy, S. M., Kroll, J. H., Ng, N. L., Hildebrandt, L., Sorooshian, A.,
871 Szmigielski, R., Vermeylen, R., Maenhaut, W., and Claeys, M.: Chemical composition of
872 secondary organic aerosol formed from the photooxidation of isoprene, *J. Phys. Chem. A*, 110,
873 9665-9690, 2006.

874 Thornton, J. A., Braban, C. F., and Abbatt, J. P. D.: N₂O₅ hydrolysis on sub-micron organic
875 aerosols: the effect of relative humidity, particle phase, and particle size, *Phys. Chem. Chem*
876 *Phys.*, 5, 4593-4603, <https://doi.org/10.1039/B307498F>, 2003.

877 Tie, X., Brasseur, G., Emmons, L., Horowitz, I., and Kinnison, D.: Effects of aerosols on
878 tropospheric oxidants: a global model study, *J. Geophys. Res. Atmos.*, 106, 22931-22964, 2001.

879 [Tong, H., Arangio, A. M., Lakey, P. S. J., Berkemeier, T., Liu, F., Kampf, C. J., Brune, W. H.,](#)
880 [Pöschl, U., and Shiraiwa, M.: Hydroxyl radicals from secondary organic aerosol decomposition](#)
881 [in water, *Atmos. Chem. Phys.*, 16, 1761-1771, doi:10.5194/acp-16-1761-2016, 2016.](#)

882 Usher, C. R., Al-Hosney, H., Carlos-Cuellar, S., and Grassian, V. H.: A laboratory study of the
883 heterogeneous uptake and oxidation of sulfur dioxide on mineral dust particles, *J. Geophys. Res.*,
884 107, 4713, doi:10.1029/2002JD002051, 2002.

885 Varutbangkul, V., Brechtel, F. J., Bahreini, R., Ng, N. L., Keywood, M. D., Kroll, J. H., Flagan,
886 R. C., Seinfeld, J. H., Lee, A., and Goldstein, A. H.: Hygroscopicity of secondary organic
887 aerosols formed by oxidation of cycloalkenes, monoterpenes, sesquiterpenes, and related

888 compounds, *Atmos. Chem. Phys.*, 6, 2367–2388, <http://www.atmos-chem-phys.net/6/23>
889 67/2006/, 2006.

890 Veghte, D. P., Altaf, M. B., and Freedman, M. A.: Size dependence of the structure of organic
891 aerosol, *J. Am. Chem. Soc.*, 135, 16046–16049, 2013.

892 Wang, G., Zhang, R., Gomez, M. E., Yang, L., Zamora, M. L., Hu, M., Lin, Y., Peng, J., Guo, S.,
893 and Meng, J.: Persistent sulfate formation from London Fog to Chinese haze, *Proc. Natl. Acad.*
894 *Sci. U. S. A.*, 113, 13630-13635, 2016.

895 Wang, S., Ye, J., Soong, R., Wu, B., Yu, L., Simpson, A. J., and Chan, A. W. H.: Relationship
896 between chemical composition and oxidative potential of secondary organic aerosol from
897 polycyclic aromatic hydrocarbons, *Atmos. Chem. Phys.*, 18, 3987-4003, 2018.

898 Wang, S., Zhou, S., Tao, Y., Tsui, W. G., Ye, J., Yu, J. Z., Murphy, J. G., McNeill, V. F.,
899 Abbatt, J. P. D., and Chan, A. W. H.: Organic peroxides and sulfur dioxide in aerosol: Source of
900 particulate sulfate, *Environ. Sci. Technol.*, 53, 10695-10704, [10.1021/acs.est.9b02591](https://doi.org/10.1021/acs.est.9b02591), 2019.

901 Wang, X.; Gemayel, R.; Hayeck, N.; Perrier, S.; Charbonnel, N.; Xu, C.; Chen, H.; Zhu, C.;
902 Zhang, L.; Wang, L.; Nizkorodov, S. A.; Wang, X.; Wang, Z.; Wang, T.; Mellouki, A.; Riva, M.;
903 Chen, J.; George, C. Atmospheric photosensitization: A new pathway for sulfate formation,
904 *Environ. Sci. Technol.*, 54, 3114-3120, 2020.

905 Wang, Y., Zhang, Q., Jiang, J., Zhou, W., Wang, B., He, K., Duan, F., Zhang, Q., Philip, S., and
906 Xie, Y.: Enhanced sulfate formation during China's severe winter haze episode in January 2013
907 missing from current models, *J. Geophys. Res. Atmos.*, 119, 10425–10440, 2014.

908 Wei, H., Vejerano, E. P., Leng, W., Huang, Q., Willner, M. R., Marr, L. C., and Vikesland, P. J.:
909 Aerosol microdroplets exhibit a stable pH gradient, *Proc. Natl. Acad. Sci. U. S. A.*, 115, 7272,
910 [10.1073/pnas.1720488115](https://doi.org/10.1073/pnas.1720488115), 2018.

911 Xu, L., Guo, H., Boyd, C. M., Klein, M., Bougiatioti, A., Cerully, K. M., Hite, J. R., Isaacman-
912 VanWertz, G., Kreisberg, N. M., and Knote, C.: Effects of anthropogenic emissions on aerosol
913 formation from isoprene and monoterpenes in the southeastern United States, *Proc. Natl. Acad.*
914 *Sci. U. S. A.*, 112, 37-42, 2015.

915 Yang, Y., Wang, H., Smith, S. J., Easter, R., Ma, P.-L., Qian, Y., Yu, H., Li, C., and Rasch, P. J.:
916 Global source attribution of sulfate concentration and direct and indirect radiative forcing,
917 *Atmos. Chem. Phys.*, 17, 8903–8922, <https://doi.org/10.5194/acp17-8903-2017>, 2017.

918 Yao, M., Zhao, Y., Hu, M., Huang, D., Wang, Y.C., Yu, J. Z., and Yan, N.: Multiphase reactions
919 between secondary organic aerosol and sulfur dioxide: kinetics and contributions to sulfate
920 formation and aerosol aging, *Environ. Sci. Tech. Let.* 6, 768-774, 2019.

921 Ye, J., Gordon, C. A., and Chan, A. W. H: Enhancement in secondary organic aerosol formation
922 in the presence of preexisting organic particle, *Environ. Sci. Technol.*, 50, 3572-3579, 2016.

923 Ye, J., Abbatt, J. P. D., and Chan, A. W. H.: Novel pathway of SO₂ oxidation in the atmosphere:
924 reactions with monoterpene ozonolysis intermediates and secondary organic aerosol, *Atmos.*
925 *Chem. Phys.*, 18, 5549–5565, <https://doi.org/10.5194/acp18-5549-2018>, 2018.

926 Yee, L. D., Isaacman-VanWertz, G., Wernis, R. A., Kreisberg, N. M., Glasius, M., Riva, M.,
927 Surratt, J. D., de Sá, S. S., Martin, S. T., Alexander, M. L., Palm, B. B., Hu, W., Campuzano-
928 Jost, P., Day, D. A., Jimenez, J. L., Liu, Y., Misztal, P. K., Artaxo, P., Viegas, J., Manzi, A., de

929 Souza, R. A. F., Edgerton, E. S., Baumann, K., and Goldstein, A. H.: Natural and
930 anthropogenically influenced isoprene oxidation in southeastern United States and central
931 Amazon, *Environ. Sci. Technol.*, 54, 5980-5991, 10.1021/acs.est.0c00805, 2020.

932 You, Y., Renbaum-Wolff, L., Bertram, A. K.: Liquid-liquid phase separation in particles
933 containing organics mixed with ammonium sulfate, ammonium bisulfate, ammonium nitrate or
934 sodium chloride, *Atmos. Chem. Phys.*, 13, 11723–11734, [https://doi.org/10.5194/acp-13-11723-](https://doi.org/10.5194/acp-13-11723-2013)
935 2013, 2013.

936 You, Y., Smith, M. L., Song, M., Martin, S. T., and Bertram, A. K.: Liquid–liquid phase
937 separation in atmospherically relevant particles consisting of organic species and inorganic salts,
938 *Int. Rev. Phys. Chem.*, 33, 43–77, doi:10.1080/0144235X.2014.890786, 2014.

939 Zhang, S., Xing, J., Sarwar, G., Ge, Y., He, H., Duan, F., Zhao, Y., He, K., Zhu, L. and Chu, B.:
940 Parameterization of heterogeneous reaction of SO₂ to sulfate on dust with coexistence of NH₃
941 and NO₂ under different humidity conditions, *Atmos. Environ.*, 208, 133-140, 2019.

942 Zhao, Y., Liu, Y., Ma, J., Ma, Q., and He, H.: Heterogeneous reaction of SO₂ with soot: The
943 roles of relative humidity and surface composition of soot in surface sulfate formation, *Atmos.*
944 *Environ.*, 152, 465-476, 2017.

945 Zheng, B., Zhang, Q., Zhang, Y., He, K. B., Wang, K., Zheng, G. J., Duan, F. K., Ma, Y. L., and
946 Kimoto, T.: Heterogeneous chemistry: a mechanism missing in current models to explain
947 secondary inorganic aerosol formation during the January 2013 haze episode in North China,
948 *Atmos. Chem. Phys.*, 15, 2031–2049, doi:10.5194/acp-15-2031-2015, 2015.

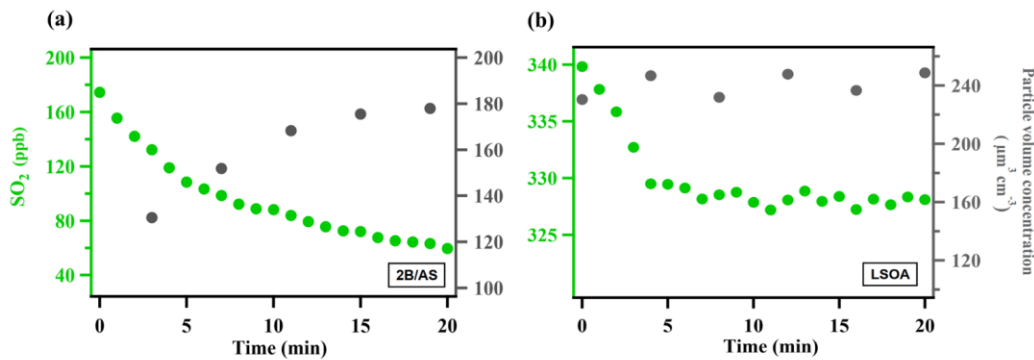
949 Zheng, G. J., Duan, F. K., Su, H., Ma, Y. L., Cheng, Y., Zheng, B., Zhang, Q., Huang, T.,
950 Kimoto, T., Chang, D., Pöschl, U., Cheng, Y. F., and He, K. B.: Exploring the severe winter haze
951 in Beijing: the impact of synoptic weather, regional transport and heterogeneous reactions,
952 *Atmos. Chem. Phys.*, 15, 2969–2983, doi:10.5194/acp-15-2969-2015, 2015.

953 [Zheng, G., Su, H., Wang, S., Andreae, M. O., Pöschl, U., and Cheng, Y.: Multiphase buffer](#)
954 [theory explains contrasts in atmospheric aerosol acidity, *Science*, 369, 1374-1377,](#)
955 [10.1126/science.aba3719, 2020.](#)

956

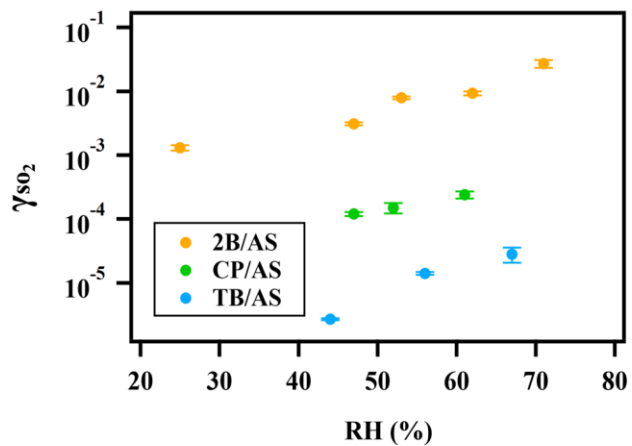
957

958



959
 960 **Figure 1.** Typical evolution of the species monitored during γ_{SO_2} measurement for (a)
 961 ammonium sulfate mixed with 2-butanone organic peroxide (2B/AS, Expt. 16) and (b) limonene
 962 SOA (LSOA, Expt. 27). Particle volume concentrations measured by SMPS have been corrected
 963 for wall loss assuming a pseudo first-order loss rate (Ye et al., 2016). γ_{SO_2} was calculated for the
 964 initial portion of the decay (first 7 minutes).

965
 966
 967
 968
 969
 970
 971
 972
 973
 974
 975



976
 977 **Figure 2.** Exponential relationship between γ_{SO_2} and RH for ammonium sulfate aerosol
 978 containing 2-butanone peroxide (2B), cumene hydroperoxide (CP), tert-butyl hydroperoxide
 979 (TB).

980

981

982

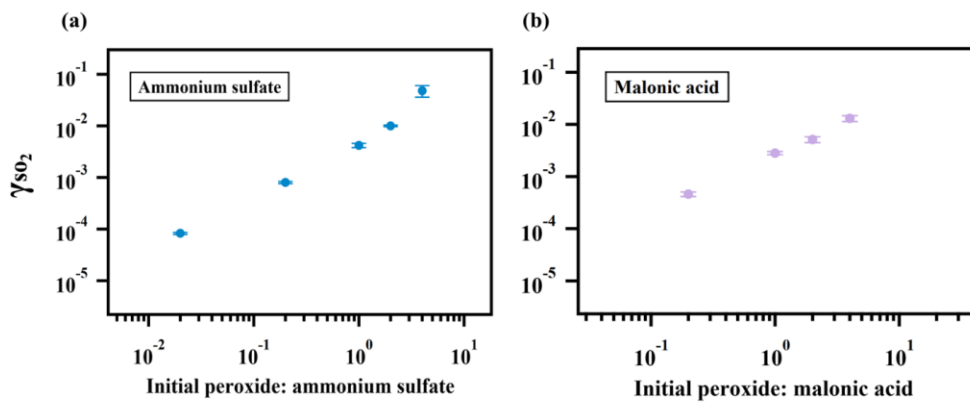
983

984

985

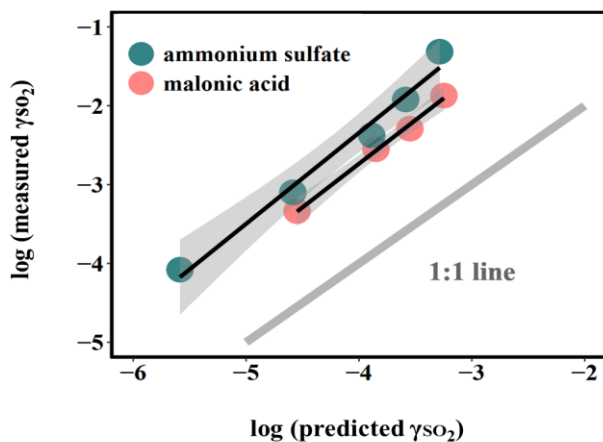
986

987



988
 989 **Figure 3.** Relationship between γ_{SO_2} and particulate peroxide content. γ_{SO_2} for ammonium sulfate
 990 (a) and malonic acid aerosol (b) containing different amount of 2-butanone peroxide are shown
 991 here. The observed dependence of γ_{SO_2} on the amount of peroxide injected are linear since the
 992 slopes of the relationship are both nearly 1 in (a) and (b).

993
 994
 995
 996
 997
 998
 999



1000

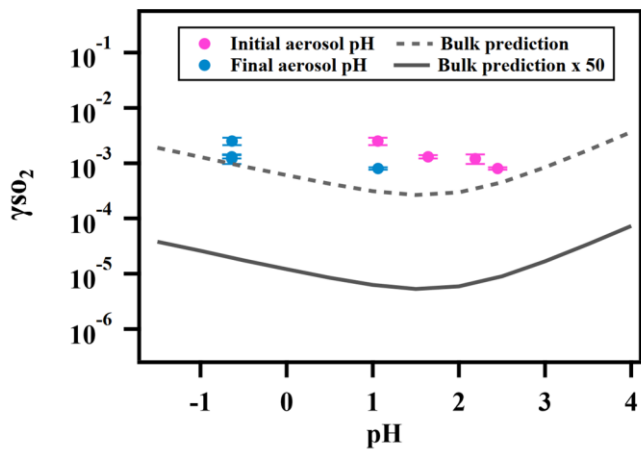
1001 **Figure 4.** Relationship between measured γ_{SO_2} and γ_{SO_2} predicted by Eqn. 5. The large deviation
 1002 from the 1:1 line, which represents the difference between the measured uptake coefficient and
 1003 predicted values based on kinetics in the dilute aqueous phase, indicates that aerosol reactive
 1004 uptake is significantly faster than reactions in dilute aqueous phase. This enhancement is likely
 1005 driven in part by high ionic strengths, as the difference between measured γ_{SO_2} and predicted γ_{SO_2}
 1006 are consistently higher for organic peroxide containing ammonium sulfate (high ionic strength)
 1007 than for that mixed with malonic acid (lower ionic strength).

1008

1009

1010

1011



1012

1013 **Figure 5.** Relationship between γ_{SO_2} and aerosol phase pH for ammonium sulfate aerosol

1014 containing 2-butanone peroxide.

1015

1016

1017

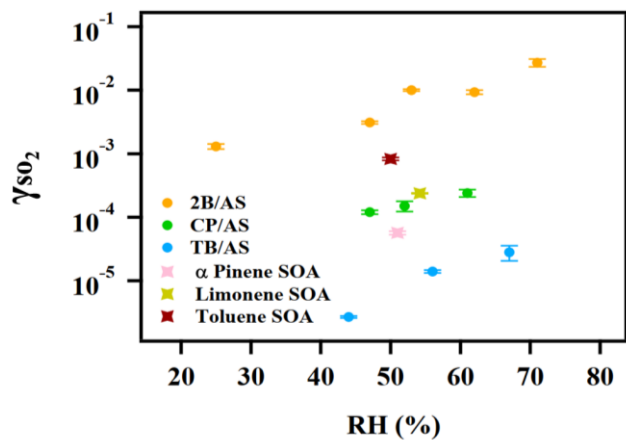
1018

1019

1020

1021

1022



1023

1024 **Figure 6.** γ_{SO_2} measured for different types of organic aerosol. The reactive uptake coefficient of
 1025 SO_2 onto SOA are on the order of 10^{-4} .

1026

1027

1028

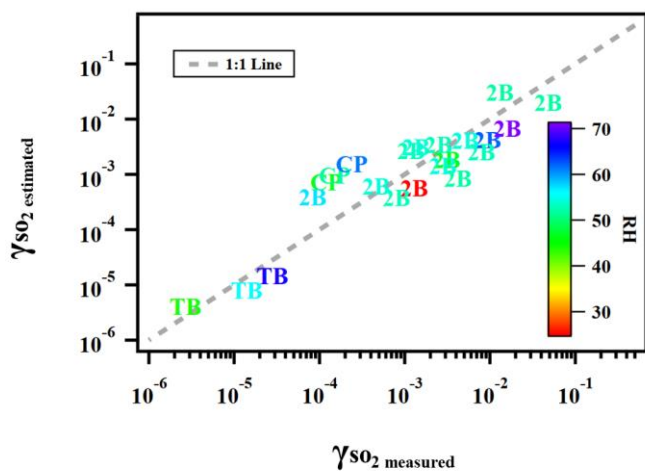
1029

1030

1031

1032

1033



1034

1035 **Figure 7.** Predicted γ_{SO_2} using Equation (13) versus measured γ_{SO_2} for ammonium sulfate or
 1036 malonic acid aerosol containing 2-butanone peroxide (2B), cumene hydroperoxide (CP), tert-
 1037 butyl hydroperoxide (TB) under different experimental conditions.

1038

1039

1040

1041

1042

1043

1044